[American Journal of Science, Vol. 316, October, 2016, P. 713–745, DOI 10.2475/08.2016.01]

American Journal of Science

*OCTOBER 2016*

# A HOLOCENE HISTORY OF DYNAMIC WATER COLUMN REDOX CONDITIONS IN THE LANDSORT DEEP, BALTIC SEA

DALTON S. HARDISTY*, NATASCHA RIEDINGER**, NOAH J. PLANAVSKY***, DAN ASAEL***, THOMAS ANDRÉN§, BO B. JØRGENSEN§§, and TIMOTHY W. LYONS*

**ABSTRACT. The modern Baltic Sea is the world's largest anthropogenically forced anoxic basin. Using integrated geochemical records collected during Integrated Ocean Drilling Program (IODP) Expedition 347 from the deepest and one of the most reducing sub-basins in the Baltic Sea, Landsort Deep, we explore the degree and frequency of natural anoxia through the Baltic Holocene. A marked decrease in carbon-to-sulfur ratios (C/S) from the cores indicate the transition from the Baltic Ice Lake to the current brackish sea, which occurred about 8.5 kyrs B.P. Following this, laminations throughout sediments recording brackish deposition suggest sustained anoxia or extreme low oxygen, while high molybdenum (Mo) concentrations of >100 ppm and iron (Fe) geochemistry suggest water column sulfide accumulation, or euxinia, that persisted beyond seasonal timescales during deposition of two distinct sapropel units. Sedimentary Mo isotope values range from +1.11 to −0.50 permil, which are distinctly fractionated from modern Baltic seawater (+2.26 to +2.67‰) and thus indicate that each of the sapropels experienced only weak and/or oscillatory euxinia—in contrast to the more stable euxinic conditions of more restricted basins. A shift in $\delta^{98}$Mo starting above the lower sapropel to a distinctly more negative range suggests particularly weak and oscillatory euxinia, with an enhanced contribution of manganese (Mn) redox cycling to Mo deposition relative to the lower portion of the profile. This conclusion is supported by extreme sedimentary Mn enrichments of up to 15 weight percent. We interpret the combined data to indicate episodic but major Baltic inflow events of saline and oxygenated North Sea water into the anoxic Landsort Deep that limited the concentrations and residence time of water column sulfide and caused episodic oxide deposition. Considering the temporal overlap between the most reducing conditions and periods of redox instability, we hypothesize that major Baltic inflows, as is observed today, lead to short-term instability while simultaneously supporting longer-term Baltic anoxia by strengthening the halocline. Ultimately, our results indicate that periods more reducing than the modern Baltic Sea have occurred naturally over the Holocene, but the characteristic dynamic saline inputs have historically prevented the relatively more widespread and stable anoxia observed in other classic restricted basins and will likely continue to do so.**

Keywords: IODP Expedition 347, Baltic Sea, Landsort Deep, paleoredox, molybdenum isotopes

## INTRODUCTION

The Baltic Sea is currently the world's largest and most variable low oxygen basin (Diaz and Rosenberg, 2008). Oxygen variation occurs on centennial, decadal, and seasonal timescales (Zillén and others, 2008; Conley and others, 2014; Carstensen and

* Department of Earth Sciences, University of California-Riverside, Riverside California 92521, USA
** Boone Pickens School of Geology, Oklahoma State University, Stillwater, Oklahoma 74074, USA
*** Department of Geology and Geophysics, Yale University, New Haven, Connecticut 06520, USA
§ School of Natural Sciences, Technology and Environmental Studies, Södertörn University, Huddinge, Sweden
§§ Center for Geomicrobiology, Department of Bioscience, Aarhus University, Aarhus C, Denmark

others, 2014), with water column redox ranging from sulfide accumulation (euxinia), in the extreme, to milder reducing conditions characterized by dissolved manganese accumulation (Dellwig and others, 2012; Carstensen and others, 2014). Today's oxygen deficiency is linked, in part, to human-induced nutrient loading together with climate change (Kabel and others, 2012), but the Baltic Sea has experienced known intervals of natural oxygen deficiency since the most recent establishment as a brackish basin ~8.5 to 8.0 thousand years ago (ka) (Boesen and Postma, 1988; Sternbeck and Sohlenius, 1997; Sternbeck and others, 2000; Sohlenius and others, 2001; Fehr and others, 2008; Zillén and others, 2008; Jilbert and Slomp, 2013; Jilbert and others, 2015). This transition was facilitated by flooding of the shallow Öresund Straits in response to rising global sea-level, which provided an additional entrance and exit for both North Sea saline marine waters and Scandinavian freshwater drainage (Zillén and others, 2008; Mohrholz and others, 2015). Together, the spatiotemporal range of observed redox states and the intermittent ventilation of oxygen-depleted bottom waters distinguish the Baltic Sea from classic modern settings of intense, persistent oxygen deficiency, such as the Black Sea and Cariaco Basin. As the world's largest anthropogenically forced oxygen-depleted basin, the Baltic Sea is more representative of the patterns of oxygen loss seen, with increasing frequency, in many coastal regions today (Diaz and Rosenberg, 2008). Currently, however, comprehensive geochemical proxy records of the full Holocene history in the Baltic are limited, thus precluding quantitative comparisons of the natural anoxic baseline relative to the current, human-impacted anoxic conditions.

The most temporally extensive Baltic sedimentary records to-date were recovered from Landsort Deep during the Integrated Ocean Drilling Program (IODP) Expedition 347 (fig. 1), capturing the transition from the glacio-lacustrine laminated clay sediments of the Baltic Ice Lake to the present laminated organic-rich Baltic Sea (Andrén and others, 2015). The Deep's distance from the sill (fig. 1) and a water depth of 459 m (the deepest Baltic sub-basin) prime it to respond relatively intensely to larger scale changes in overall long-term Baltic redox conditions (Carstensen and others, 2014). A detailed reconstruction of Holocene redox transitions and a comparison of the degree (euxinic > ferruginous > manganeous > oxygenated) and frequency (semi-permanent > oscillatory > seasonal) of reducing conditions relative to those observed today would be a key step toward unraveling the processes that regulate Baltic oxygen depletion. Herein, we employ a series of geochemical proxies that are progressively sensitive to specific redox regimes—manganese, iron, and molybdenum—to reconstruct a high-resolution history of redox transitions in the Landsort Deep.

## BACKGROUND

### *Baltic Basin*

The Baltic Basin has experienced dynamic physical and chemical oceanographic conditions since the Late Weichselian deglaciation. Following the last glacial maximum about 22 ka, the Baltic ice lobe, which extended over the Öresund Strait into Denmark and covered the Baltic Sea since 55 ka, began retreating north (Andrén and others, 2011). The freshwater Baltic Ice Lake formed at ~16 ka as glacial melt water from the retreating ice sheet filled the Baltic basin. At the same time, ice blockage and isostatic rebound from ice retreat across the Öresund Strait severed any connection to the North Sea (Houmark-Nielsen and Henrik Kjaer, 2003; Björck, 2008; Andrén and others, 2011). Around 11.7 ka (Walker and others, 2009), the dam was breached and the Baltic Ice Lake drained into the North Sea, with estimates for the drop in lake level reaching 25 m over a period of as little as 1 to 2 years (Björck and others, 1996; Jakobsson and others, 2007). The resulting Yoldia Sea formed a brief and weak

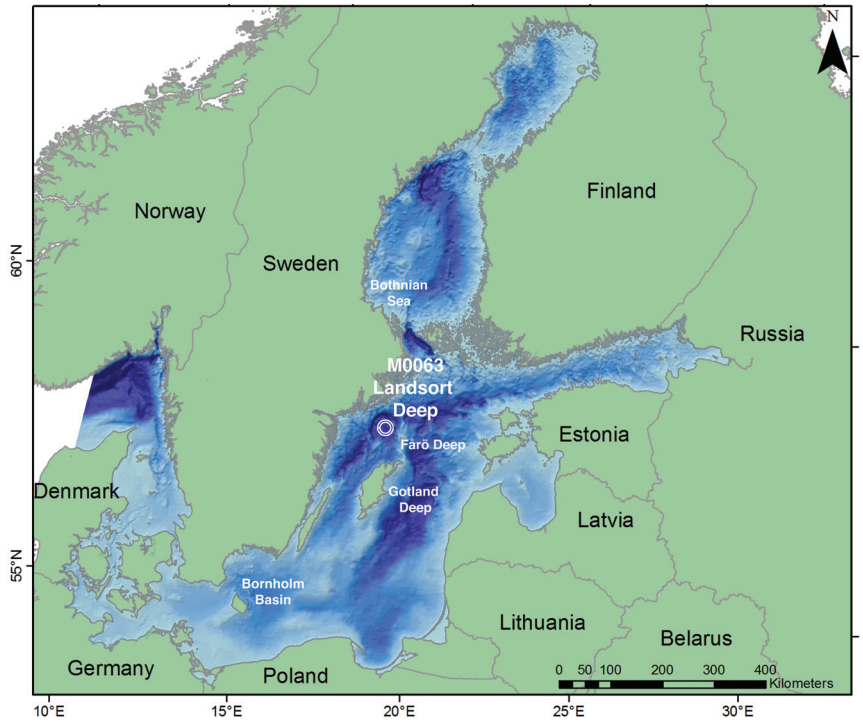


Fig. 1. Baltic Sea map showing IODP Expedition 347 site M0063, or Landsort Deep, the focus of this study.

connection to the North Sea perhaps for only 350 years (Andrén and Sohlenius, 1995; Wastegård and others, 1995; Andén and others, 2007). Then, isostatic rebound again dammed the Baltic Basin from the open ocean by 10.7 ka, forming the Ancylus Lake (Andrén and others, 2011). Beginning at 9.8 ka (Andrén and others, 2000a; Andrén and others, 2000b; Berglund and others, 2005; Andrén and others, 2011), eustatic sea level rise from the melting Antarctic and Laurentide ice sheets (Lambeck and Chappell, 2001) gradually flooded the Danish straights. Later, at 8.5 to 8.0 ka, the Öresund Strait flooded, establishing the brackish Littorina Sea stage, which lasted until 3.0 ka (Björck and others, 2008). The following 1.5 ka, or Post-Littorina stage, was characterized by a declining salinity and onset of the modern silled Baltic system (Sohlenius and others, 1996; Sohlenius and Westman, 1998; Andrén and others, 2000a). Today, saline waters from the North Sea enter and exit the basin through the narrow and shallow Danish straights, with a present mean water depth of ~20 and 11 meters in the Great Belt and Öresund Strait, respectively (Mohrholz and others, 2015).

Three main periods of Holocene low oxygen conditions are inferred from the presence of laminated sediments at *ca.* 8.0 to 4.0 ka, 2.0 to 0.8 ka, and over the last 200 years (Zillén and others, 2008). These periods correspond roughly with the Holocene Thermal Maximum (HTM; ~9.0–5.0 ka ago), the Medieval Climate Anomaly (MCA; ~1.2–0.8 ka), and the modern historical period (Zillén and others, 2008)—with past anoxia linked to salinity changes and varying freshwater inputs into the basin during the HTM (Middleburg, 1991; Gustafsson and Westman, 2002; Conley and others, 2009) and warmer temperatures associated with the MCA (Kabel and others, 2012). Unlike the first two intervals of oxygen depletion, the most recent period is clearly

attributable to human activities in the region in combination with a warmer climate (Kabel and others, 2012; Carstensen and others, 2014). Increased nutrient discharge from expanding agriculture and industrialization in response to increased population and the industrial revolution amplified eutrophication and resulted in the expansion of oxygen-depleted bottom waters. There are sediment laminations and redox sensitive trace metal enrichments in sediments beginning roughly with the onset of the 19$^{th}$ century (Zillén and others, 2008), and direct water column measurements record oxygen depletion near the beginning of the 20$^{th}$ century (Carstensen and others, 2014). Studies suggest that the onset of reducing conditions occurred more rapidly for the current anoxic era relative to those of the past (Jilbert and Slomp, 2013), which was followed by a tenfold increase in the area of reducing bottom waters over the last century (Carstensen and others, 2014).

Today, these is a lateral salinity gradient from south to north, with surface salinity near 8 to 10 PSU in the southern Baltic and 3 to 5 PSU to the north in the Gulf of Finland (Matthäus, 2006), and a vertical gradient of ~4 to 5 PSU in the Baltic proper. Circulation of seawater in and out of the Baltic occurs as a gyre trending counterclockwise through the basin (Döös and others, 2004). In the Landsort Deep, the focus of this study, the resulting halocline is at ~80 m water depth (Dellwig and others, 2012). Sporadic but substantial incursions of marine water from the North Sea, termed major Baltic inflows (MBIs), are barotropic events driven by special conditions of large-scale atmospheric circulation over the North Atlantic (Mohrholz and others, 2015). These MBIs drive bottom-water oxygenation events, providing oxygen-rich and saline North Sea waters to formerly anoxic waters of the Baltic deeps (Carstensen and others, 2014). At the same time, introduction of these saline bottom waters maintains long-term Baltic anoxia by strengthening the halocline (Carstensen and others, 2014). The average residence time of Baltic water today is ~30 years (Stigebrandt and Gustafsson, 2003; Döös and others, 2004), but this estimate varies with distance from the sill (Carstensen and others, 2014). Today, Landsort Deep is a euxinic basin with dissolved sulfide concentrations of <13.5 μM (Nägler and others, 2011; Dellwig and others, 2012), and MBIs occur on decadal timescales (Carstensen and others, 2014). The latest MBI occurred in late 2014 and was the third strongest since 1880 (Mohrholz and others, 2015).

### *Geochemical Techniques*

*Iron proxies.*—The amount of 'highly reactive' mineral-bound Fe ($Fe_{HR}$) in sediments, defined as being reactive with hydrogen sulfide on short diagenetic time scales, relative to the amount of total Fe ($Fe_T$) can be used to identify anoxic conditions in modern and ancient water columns (Raiswell and Canfield, 1998). Furthermore, the extent to which the $Fe_{HR}$ has been sulfidized to form pyrite ($Fe_{py}$) allows us to distinguish between ferruginous and euxinic conditions (Canfield and others, 1992; Raiswell and Canfield, 1998; Poulton and Canfield, 2005). $Fe_{HR}$ is typically defined as the sum of Fe bound in amorphous and crystalline Fe(oxyhydr)oxides, siderite, Fe monosulfides, and pyrite. Under anoxic conditions, an enhanced input of $Fe_{HR}$ can be decoupled from the typical detrital input, leading to ratios that exceed the upper detrital limit recognized as 0.38 (Raiswell and Canfield, 1998) and $Fe_T/Al$ ratios beyond the detrital baseline of ~0.4 to 0.6 (Lyons and Severmann, 2006). If dissolved sulfide is persistently available in the water column, syngenetic iron sulfide typically leads to $Fe_{py}/Fe_{HR}$ ratios of greater than 0.8 (Canfield and others, 1996; Poulton and Canfield, 2011). From these observations, the combination of $Fe_{HR}/Fe_T > 0.38$, $Fe_T/Al > 0.4$ to 0.6, and $Fe_{py}/Fe_{HR} > 0.8$ is commonly used to infer euxinic conditions, and this approach has proven utility throughout the geologic record (Poulton and Canfield, 2011). Though not yet observed in modern marine settings, indications of anoxia in the water column combined with $Fe_{py}/Fe_{HR}$ ratios of <0.8 suggest that availability of

water column sulfide is limiting pyrite formation, thus suggesting iron-rich or ferruginous conditions (Canfield and others, 2008; Poulton and Canfield, 2011).

*Molybdenum and manganese proxies.*—Molybdenum is the most abundant transition metal in the modern ocean with a concentration of ~104 nM (Miller and others, 2011); however, due to its brackish salinity, concentrations in the Baltic Sea are closer to 20 nM (Neubert and others, 2008; Noordmann and others, 2015). The primary Mo species under oxic conditions is molybdate ($MoO_4^{2-}$), which has an affinity for adsorption to Mn and Fe oxides—the main pathway of Mo deposition to sediments in the modern ocean (Barling and Anbar, 2004). However, under sulfide-rich conditions, $MoO_4^{2-}$ is converted to particle reactive thiomolybdates ($MoO_{4-x}S_x^{2-}$) (Erickson and Helz, 2000) and reactive Mo-polysulfide species (Dahl and others, 2013) and is efficiently buried—frequently in association with organic matter (Algeo and Lyons, 2006). In euxinic water columns with >100 μM persistent total dissolved sulfide accumulation, high sedimentary Mo enrichments of >25 ppm and often >100 ppm point uniquely to stably euxinic conditions (Scott and Lyons, 2012). Enrichments at the low end of this range can occur when connection to the open ocean is restricted, as in the modern Black Sea, and uptake and burial can be nearly quantitative (Erickson and Helz, 2000). Comparatively low Mo concentrations (<25 ppm), but above average crustal values (~2 ppm), typically reflect burial coupled to Mn/Fe oxides and are diagnostic of a non-euxinic water column (Scott and Lyons, 2012). Furthermore, sediments underlying water columns with high and stable water column sulfide concentrations can record the Mo isotope composition of contemporaneous seawater, which today is ~2.4 permil, because these systems experience near-quantitative tetrathiomolybdate formation and consequent Mo uptake and burial (Siebert and others, 2003). This relationship is observed in the modern Black Sea (Neubert and others, 2008).

During conversion of $MoO_4^{-2}$ to tetrathiomolybdate, a large isotope fractionation can be seen among the transient intermediate species (Tossell, 2005), which can be as high as −3.1 permil (Azrieli-Tal and others, 2014). This effect can result in sedimentary Mo isotope data that are negatively fractionated beneath waters with unstable euxinia with total dissolved sulfide concentrations of <100 μM (Neubert and others, 2008; Azrieli-Tal and others, 2014). Diagnostic negative Mo isotope fractionations as large as −2.9 permil (Barling and others, 2001; Wasylenki and others, 2008) and −2.2 permil (Goldberg and others, 2009) are also associated with Mo adsorption to Mn and Fe oxides, respectively.

## *Sampling and Lithological Descriptions*

Because details for the coring protocols and lithologic descriptions for IODP Expedition 347 are published elsewhere (Andrén and others, 2015), we provide only a summary below (stratigraphic column in fig. 2). Relevant intervals for Holes C and E of site M0063, Landsort Deep, were cored using an advanced piston-coring device. The lithology at site M0063 was divided into seven units and multiple subunits. Unit I (Hole C 0–25.9 mbsf) captures the brackish conditions of the Littorina Sea and the Baltic Sea since the most recent connection to the open ocean and is generally organic-rich and black in color. Laminations are present throughout Unit I in all intervals and are particularly prominent from 4.1 to 6.7 mbsf and 17.8 to 25.9 mbsf. Units II (Hole C 25.9–34.24 mbsf) and III (Hole C 34.24–41.5 mbsf) contain Ancylus Lake sediments and are defined by a dark gray color, Liesegang bands (which were avoided during sampling), and a series of basin slumping events. Unit IV (Hole C 41.5–48.62 mbsf) is interpreted, based on the presence of diatoms from 41 to 43 mbsf relative to their absence in surrounding sediments, as recording a weak brackish phase—most probably the Yoldia Sea. Similar to Units II and III, Unit IV is gray in color with black FeS bands. Units V and VI (Hole C 48.62–92.16 mbsf) are similarly gray to brown in color,

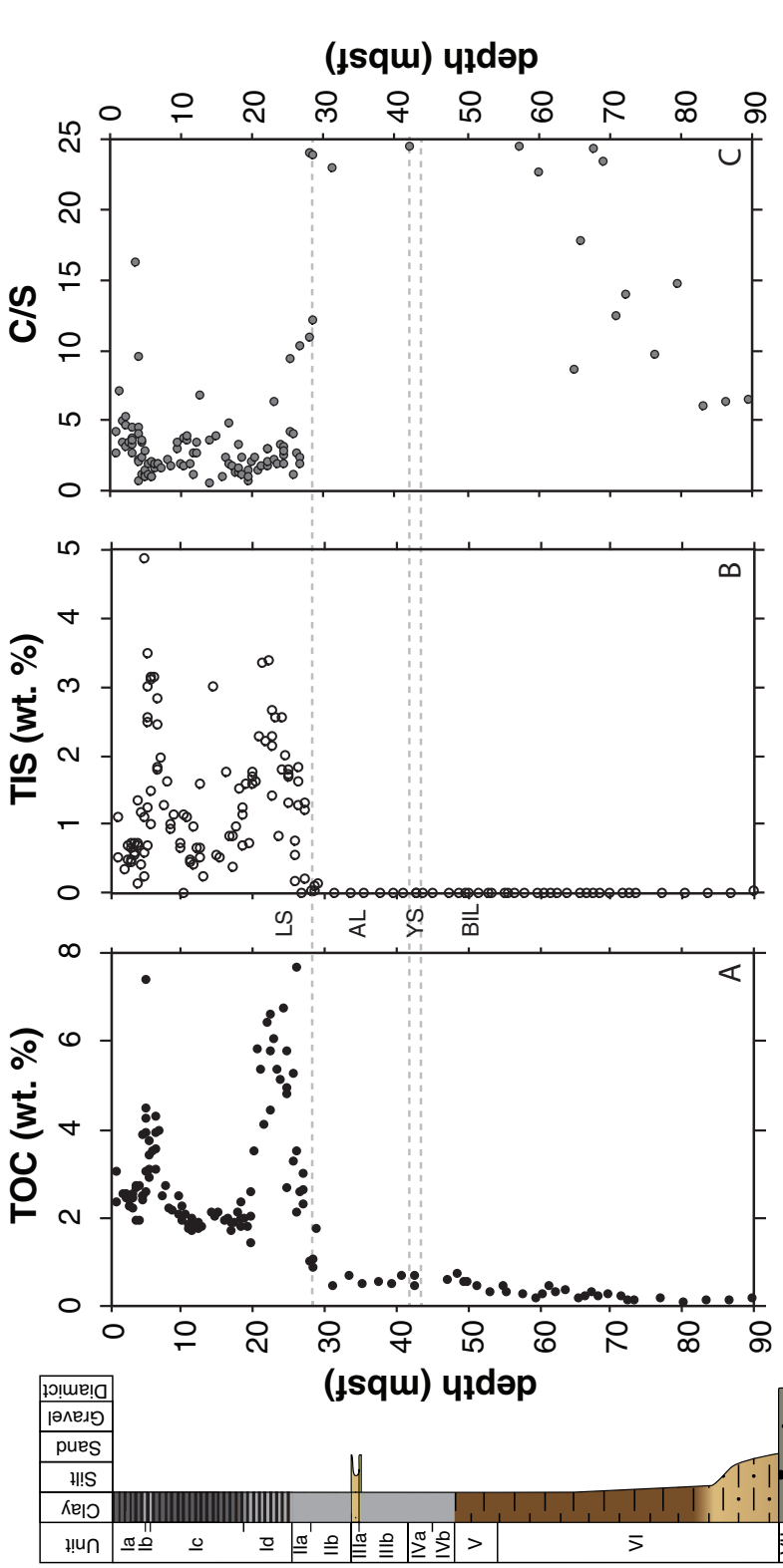


Fig. 2. M0063 down core profiles of (A) total organic carbon (TOC), (B) total inorganic sulfur (TIS), which is the sum of CRS and AVS, and (C) total organic carbon-to-inorganic sulfur (C/S) ratios. C/S ratios below 30 mbsf often exceed 25. The dashed lines separate the Baltic Ice Lake (BIL), Yoldia Sea (YS), Ancylus Lake (AL), and Baltic Sea, as inferred from the sedimentological descriptions in the M0063 summary (Andrén and others, 2015). Sediment depth is displayed as meters below sea floor (mbsf). Stratigraphic column is adapted from Andrén and others, (2015), and stresses the laminations and color changes described in the *Samples and Lithologic Descriptions* section of this manuscript.

but in this case show a distinct pattern of fining-upward rhythmic couplets interpreted to reflect a transition from ice-distal to ice-proximal glacio-lacustrine settings likely within the Baltic Ice Lake and marked by possible slumping events. Unit VII (92.16–93.30 mbsf) consists of angular, poorly sorted, pebble-sized clasts in a sandy diamicton resulting from deposition as debris flows or subglacial till (Andrén and others, 2015).

## METHODS

Samples from Hole E were collected and sealed in $N_2$-flushed bags onboard the ship immediately following collection and stored frozen prior to analysis. Cores from Hole C were capped and sealed immediately following retrieval and stored at 4 °C prior to sample collection, which occurred 4 to 5 months later at MARUM in Bremen, Germany. At Bremen, samples were collected within a few hours of core splitting and immediately sealed in $N_2$ flushed bags and stored frozen prior to analyses, minimizing oxidation of redox sensitive Fe minerals important for this study. Sediment analyses took place at the University of California-Riverside and Yale University. Fresh material was used exclusively for each analysis described below; sediments showing signs of oxidation (graying or browning from the formerly black color of iron monosulfides) were scraped away.

We used classic methods for extraction of iron monosulfide or acid volatile sulfide (AVS) (Berner and others, 1979; Chanton and Martens, 1985; Morse and Cornwell, 1987; Lyons, 1997; Hurtgen and others, 1999) and chromium reducible sulfur (CRS) (Canfield and others, 1986), in each case using a split of freshly thawed sample. Concentrations of both CRS and AVS were measured via the methylene blue method using a spectrophotometer at wavelength of 660 nm (Cline, 1969). Assuming negligible concentrations of [$S^0$], pyritic sulfur was determined by subtracting the AVS from CRS. In a few samples, likely due to heterogeneities and incomplete mixing, AVS concentrations slightly exceed those determined for CRS from the same sample. In such cases, pyritic sulfur was recorded as zero, though we acknowledge that this is unlikely to be the case. Iron present as AVS and CRS was calculated from the measured S concentrations using the stoichiometries FeS and $FeS_2$, respectively. These calculated Fe contents are represented throughout the text as $Fe_{AVS}$ and $Fe_{py}$.

To further characterize the Fe pools present, a modified chemical extraction method was used: $MgCl_2$, ascorbate ($Fe_{asc}$), dithionite ($Fe_{dith}$), oxalate ($Fe_{ox}$) and Na-acetate ($Fe_{NaAc}$) representing sorbed Fe, labile Fe oxides, crystalline Fe oxides, magnetite, and Fe carbonates, respectively (Ferdelman, ms, 1988; Kostka and Luther, 1994; Raiswell and others, 1994; Poulton and Canfield, 2005; Raiswell and others, 2010). In each case, the chemical reagents were deoxygenated with $N_2$ for >15 minutes prior to addition to the sample, and the headspace of each centrifuge tube was replaced with $N_2$ prior to shaking. Only fresh and wet—not dried powdered sediment (Raiswell and others, 1994; Raiswell and others, 2010)—was used, and sample exposure time to the atmosphere was limited to minutes during initial weighing and subsequent reagent additions. Powdering sediment samples has been shown previously to increase the $Fe_{dith}$ extractable fraction explicitly, likely due to the increase in surface area (Raiswell and others, 1994). For our purposes, this step would artificially inflate the $Fe_{dith}$ fraction and likely other oxide fractions relative to that naturally available for reaction with dissolved sulfide to form iron sulfides. Subsamples for individual analyses were carefully homogenized, but the bulk sample was kept heterogeneous in order to avoid mixing of oxidized and un-oxidized portions of the sample.

Details for the sequential Fe chemical extraction scheme follow: (1) ascorbate at pH 7.5 for 24 hours, (2) dithionite at pH 4.8 for 2 hours, and (3) oxalate at pH of 3.2 for 6 hours. Furthermore, a fresh sediment sample was used for two separate extractions: (1) $MgCl_2$ at pH 7.05 for 24 hours and (2) Na-acetate extraction at pH 4.5 for 24 hours (Poulton and Canfield, 2005). All Fe extracts were quantified via an Agilent

7500c quadrupole inductively coupled plasma-mass spectrometer (ICP-MS) upon dilution with 0.24 M nitric acid. An initial survey of all samples collected onboard the ship from Hole E (thus minimizing the likelihood of oxidation) revealed that concentrations for $MgCl_2$-extracted Fe were all below the detection limit; this step was omitted from subsequent extraction series. Separate sub-sample duplicates assessed for precision revealed relative whole analysis standard deviations in most cases <0.01 weight percent, but in a few cases <0.1 weight percent; we point out, however, that heterogeneities are expected, as bulk samples were not homogenized prior to taking a sub-sample for the sequential Fe-extraction procedure.

A separate aliquot of fresh, wet sample was removed at the same time as the split for the Fe sequential extraction scheme and dried at 60 °C for the determination of water content. Iron concentration data are reported on dry sediment basis. Due to the low salinity, dry sediment weight was not salt corrected. This dried sediment split was then homogenized and used for measurements of each total carbon, total inorganic carbon (TIC), and a total acid digest for major and trace metal analyses. Total carbon was determined using an Eltra CS-500 carbon-sulfur analyzer. Total inorganic carbon determinations were made measuring $CO_2$ concentrations from carbon liberated during an addition of 2.5 N HCl to the sample. Total organic carbon (TOC) was determined by difference of the total carbon and total inorganic carbon. The geostandard AR4007 was analyzed routinely, with values within reported ranges and deviating by <5 percent.

A multi-acid digest procedure was used for determination of bulk sediment metal concentrations. Dried samples were ashed at 450 to 650 °C and digested using trace metal grade HF:$HNO_3$:HCl, with the metals solubilized at the end in 0.24 M $HNO_3$ acid. Total digests were measured for major elements (Al, Fe, Mn) and trace elements (Mo) via an Agilent 7500c quadrupole ICP-MS using a multi-element standard solution in a 0.24 M $HNO_3$ matrix. Total digest geostandards (NIST 2702, USGS SCO-1, and USGS SGR-1) were routinely compared for accuracy, with all elements analyzed deviating by <5 percent from the reported values. All values for Al, Fe, Mn, Mo, $Fe_{asc}$, $Fe_{dith}$, $Fe_{ox}$, $Fe_{NaAc}$, $Fe_{AVS}$, $Fe_{CRS}$, TOC, and TIC can be found in table 1.

Molybdenum isotope measurements were performed at the Metal Geochemistry Center at Yale University, New Haven, Connecticut. The resulting 0.24 M $HNO_3$ solution from total digest was evaporated and re-constituted in 7 M HCl. An aliquot of the acid split was doped with a Mo double spike according to the Mo concentration determined previously via ICP-MS in order to maintain a constant sample-to-spike ratio. This aliquot was also used for chromatographic separation. The $^{97}$Mo-$^{100}$Mo double spike solution was prepared gravimetrically from Oak Ridge Laboratory metal powders as previously described (Asael and others, 2013). A two-stage column procedure was applied for Mo purification: the sample was run through an anion resin (AG-MP-1M) to separate Mo and Fe from the matrix followed by purification through a cation resin (AG50W-X8) to separate Mo from any remaining Fe. Molybdenum isotope compositions are reported using the δ notation, where:

$$\delta^{98}\mathrm{Mo}\ (‰) = 1000 \cdot [(^{98}\mathrm{Mo}/^{95}\mathrm{Mo})_{\mathrm{sample}}/(^{98}\mathrm{Mo}/^{95}\mathrm{Mo})_{\mathrm{NIST}} * 0.99975 - 1]. \quad (1)$$

$\delta^{98}$Mo is calculated relative to NIST 3134 (Lot 130418) with a value of −0.25 permil (Nägler and others, 2014). A calibration of the NIST standard relative to Rochester (Lot 862309E) gave:

$$\delta^{98}\mathrm{Mo}_{\mathrm{ROCH}} = \delta^{98}\mathrm{Mo}_{\mathrm{NIST3137}} - 0.32 \pm 0.12\ ‰. \quad (2)$$

For each sample, the target Mo concentration was 200 ppb during MC-ICP-MS analysis. For nearly all samples, the 1σ was <0.05 permil. Duplicates (n = 5) of reference

TABLE 1

*Values for Al, Fe, Mn, Mo, $Fe_{asc}$, $Fe_{dith}$, $Fe_{ox}$, $Fe_{NaAc}$, $Fe_{AVS}$, $Fe_{CRS}$, TOC, and TIC*

| Depth (mbsf) | TOC wt.% | TIC wt.% | TOC / TIS | $Fe_{asc}$ wt.% | $Fe_{dith}$ wt.% | $Fe_{ox}$ wt.% | $Fe_{NaAc}$ wt.% | $Fe_{py}$ wt. % | $Fe_{AVS}$ wt. % | $Fe_{HR}$ / $Fe_T$ | $(Fe_{py}+Fe_{AVS})$ / $Fe_{HR}$ | Mn wt % | Al wt.% | $Fe_T$ wt.% | Mo ppm |
|---|---|---|---|---|---|---|---|---|---|---|---|---|---|---|---|
| **0.70** | 3.08 | 0.00 | 2.73 | 0.27 | 0.11 | 0.39 | 0.89 | 0.00 | 1.96 | 0.66 | 0.54 | 1.72 | 8.06 | 5.46 | 13.65 |
| **0.87** | 2.36 | 0.06 | 4.34 | 0.09 | 0.03 | 0.16 | 0.47 | 0.14 | 0.67 | 0.29 | 0.56 | 0.71 | 8.28 | 5.02 | 5.56 |
| **1.47** | 2.56 | 0.04 | 7.20 | 0.16 | 0.00 | 0.19 | 0.63 | 0.00 | 0.62 | 0.28 | 0.43 | 0.32 | 8.08 | 5.10 | 4.55 |
| **1.81** | 2.53 | 0.01 | 5.00 | 0.08 | 0.04 | 0.21 | 0.46 | 0.40 | 0.08 | 0.23 | 0.42 | 0.26 | 8.03 | 5.10 | 2.33 |
| **2.04** | 2.46 | 0.03 | 3.53 | 0.14 | 0.03 | 0.12 | 0.84 | 0.60 | 0.02 | 0.33 | 0.39 | 0.30 | 7.71 | 4.92 | 3.30 |
| **2.30** | 2.45 | 0.00 | 5.42 | 0.22 | 0.05 | 0.54 | 0.41 | 0.05 | 0.69 | 0.38 | 0.38 | 0.26 | 8.41 | 5.11 | 4.64 |
| **2.37** | 2.28 | 0.01 | 4.70 | 0.14 | 0.05 | 0.19 | 0.37 | 0.00 | 0.85 | 0.29 | 0.60 | 0.27 | 8.11 | 5.06 | 3.55 |
| **2.42** | 2.40 | 0.02 | 3.27 | 0.08 | 0.04 | 0.13 | 0.67 | 0.32 | 0.64 | 0.34 | 0.54 | 0.17 | 8.11 | 5.23 | 3.57 |
| **2.56** | 2.28 | 0.02 | 3.47 | 0.08 | 0.03 | 0.18 | 0.45 | 0.47 | 0.21 | 0.25 | 0.52 | 0.21 | 8.55 | 5.26 | 1.82 |
| **2.97** | 2.55 | 0.09 | 4.61 | 0.14 | 0.07 | 0.23 | 0.66 | 0.31 | 0.34 | 0.22 | 0.42 | 0.38 | 7.87 | 7.27 | 37.30 |
| **3.05** | 2.46 | 0.00 | 3.34 | 0.12 | 0.06 | 0.39 | 0.41 | 0.56 | 0.16 | 0.33 | 0.42 | 0.15 | 8.79 | 5.11 | 6.58 |
| **3.08** | 2.25 | 0.02 | 3.80 | 0.07 | 0.04 | 0.11 | 0.48 | 0.15 | 0.72 | 0.30 | 0.60 | 0.26 | 8.03 | 5.03 | 2.53 |
| **3.34** | 1.95 | 0.81 | 2.74 | 0.14 | 0.13 | 0.30 | 1.00 | 0.43 | 0.37 | 1.00 | 0.38 | 0.33 | 0.94 | 0.66 | 0.80 |
| **3.37** | 2.71 | 0.00 | 3.71 | 0.11 | 0.05 | 0.11 | 0.33 | 0.41 | 0.46 | 0.26 | 0.67 | 0.12 | 8.46 | 5.22 | 6.03 |
| **3.55** | | 7.56 | | 0.46 | 0.23 | 0.35 | 0.62 | 0.45 | 1.49 | 0.51 | 0.67 | 9.29 | 9.06 | 6.19 | 9.41 |
| **3.59** | 2.71 | 0.18 | 16.30 | 0.08 | 0.00 | 0.16 | 0.11 | 0.12 | 0.05 | 0.08 | 0.39 | 1.20 | 7.90 | 5.47 | 9.77 |
| **3.91** | 1.93 | 0.07 | 4.66 | 0.23 | 0.07 | 0.29 | 0.62 | 0.01 | 0.71 | 0.31 | 0.44 | 0.37 | 8.42 | 5.54 | 5.09 |
| **3.99** | 2.73 | 0.00 | 2.28 | 0.21 | 0.06 | 0.30 | 1.22 | 1.03 | 0.02 | 0.47 | 0.41 | 0.13 | 7.93 | 5.63 | 5.50 |
| **4.15** | 2.51 | 0.06 | 4.13 | 0.13 | 0.04 | 0.28 | 0.39 | 0.19 | 0.68 | 0.29 | 0.57 | 0.35 | 8.51 | 5.48 | 6.75 |
| **4.21** | 2.52 | 0.00 | 9.69 | 0.32 | 0.15 | 0.39 | 0.33 | 0.22 | 0.01 | 0.20 | 0.24 | 0.21 | 8.63 | 5.57 | 9.53 |
| **4.30** | 3.87 | 0.02 | 0.79 | 0.70 | 1.23 | 0.34 | 2.99 | 3.29 | 1.90 | 1.00 | 0.61 | 0.21 | 4.11 | 5.89 | 68.54 |
| **4.31** | 2.42 | 0.00 | 2.15 | 0.04 | 0.15 | 0.21 | 0.15 | 0.83 | 0.31 | 0.30 | 0.76 | 0.18 | 8.11 | 5.54 | 5.93 |
| **4.56** | 4.27 | 3.65 | 1.22 | 0.11 | 1.23 | 0.20 | 0.31 | 2.75 | 0.57 | | 0.87 | | 0.00 | 0.00 | 0.00 |
| **4.59** | 4.47 | 2.80 | 3.54 | 0.17 | 0.07 | 0.25 | 0.54 | 0.90 | 0.40 | 0.40 | 0.62 | 0.76 | 7.65 | 5.43 | 14.27 |
| **4.60** | 2.57 | 0.00 | 3.69 | 0.12 | 0.05 | 0.45 | 0.62 | 0.34 | 0.54 | 0.41 | 0.41 | 0.10 | 7.87 | 5.21 | 4.80 |
| **4.62** | 7.38 | 0.00 | 2.44 | 0.13 | 0.04 | 0.14 | 0.26 | 2.57 | 0.13 | 0.53 | 0.83 | 0.27 | 6.60 | 6.11 | 98.70 |
| **4.83** | 3.06 | 0.12 | 1.20 | 0.33 | 0.74 | 0.21 | 0.63 | 1.19 | 2.07 | 1.00 | 0.80 | 13.78 | 3.80 | 4.13 | 79.57 |
| **4.85** | 3.92 | 0.02 | 1.57 | 0.36 | 0.38 | 0.18 | 0.99 | 1.93 | 0.49 | 0.86 | 0.68 | 9.29 | 5.54 | 4.61 | 57.15 |
| **5.06** | 2.90 | 0.00 | 2.91 | 0.10 | 0.14 | 0.23 | 0.46 | 0.85 | 0.03 | 0.33 | 0.56 | 7.83 | 9.57 | 5.20 | |
| **5.15** | 3.41 | 3.42 | 1.08 | 0.12 | 0.71 | 0.29 | 0.27 | 1.44 | 2.63 | 1.00 | 0.88 | 11.77 | 3.60 | 3.50 | 85.51 |
| **5.31** | 3.10 | 0.00 | 2.05 | 0.09 | 0.02 | 0.17 | 0.12 | 1.28 | 0.07 | 0.35 | 0.83 | 0.00 | 8.08 | 4.78 | |
| **5.41** | 3.74 | 0.04 | 1.20 | 0.51 | 0.57 | 0.17 | 1.70 | 1.01 | 3.40 | 1.00 | 0.70 | 0.00 | 3.06 | 3.84 | 91.01 |
| **5.67** | 3.50 | 2.41 | 1.11 | 0.09 | 1.09 | 0.23 | 0.71 | 2.45 | 0.61 | 1.00 | 0.76 | 9.31 | 4.52 | 4.77 | 11.44 |

Table 1

*(continued)*

| Depth (mbsf) | TOC wt.% | TIC wt.% | TOC / TIS | $Fe_{asc}$ wt.% | $Fe_{dith}$ wt.% | $Fe_{ox}$ wt.% | $Fe_{NaAc}$ wt.% | $Fe_{py}$ wt. % | $Fe_{AVS}$ wt. % | $Fe_{HR}$ / $Fe_T$ | $(Fe_{py}+Fe_{AVS})$ / $Fe_{HR}$ | Mn wt % | Al wt.% | $Fe_T$ wt.% | Mo ppm |
|---|---|---|---|---|---|---|---|---|---|---|---|---|---|---|---|
| **5.94** | 3.91 | 0.04 | 2.10 | 0.07 | 0.16 | 0.09 | 0.65 | 1.06 | 1.11 | 0.90 | 0.75 | 14.07 | 3.82 | 3.39 | 127.49 |
| **6.05** | 3.12 | 0.01 | 1.09 | 0.44 | 0.35 | 0.19 | 1.58 | 1.30 | 2.38 | 1.00 | 0.67 | 14.97 | 6.26 | 5.27 | 73.93 |
| **6.13** | 4.28 | 3.34 | 1.75 | 0.11 | 1.14 | 0.35 | 0.88 | 1.91 | 0.45 | 1.00 | 0.66 | 14.13 | 2.73 | 3.73 | 27.47 |
| **6.23** | 3.57 | 3.95 | 1.97 | 0.17 | 0.64 | 0.25 | 0.38 | 1.24 | 0.67 | 0.97 | 0.75 | 14.71 | 3.43 | 3.29 | 27.63 |
| **6.80** | 3.97 | 3.31 | 1.99 | 0.08 | 0.84 | 0.38 | 0.13 | 1.38 | 0.72 | 1.00 | 0.80 | 11.51 | 3.51 | 3.39 | 40.00 |
| **6.88** | 2.49 | 0.00 | 1.95 | 0.20 | 0.11 | 0.24 | 0.43 | 1.10 | 0.01 | 0.32 | 0.62 | 6.18 | 8.54 | 5.85 | 9.46 |
| **7.34** | 2.75 | 0.02 | 1.67 | 0.42 | 0.16 | 1.36 | 1.74 | 0.69 | 1.50 | 0.99 | 0.37 | 6.81 | 4.83 | 5.93 | 36.74 |
| **8.03** | | 0.24 | | 0.29 | 0.17 | 0.44 | 0.81 | 0.59 | 0.57 | 0.43 | 0.48 | 0.45 | 8.76 | 5.97 | 19.75 |
| **8.13** | 2.25 | 0.11 | 2.35 | 0.00 | 0.49 | 0.36 | 0.62 | 0.55 | 0.56 | 0.45 | 0.53 | 0.63 | 8.35 | 5.69 | 4.29 |
| **8.48** | 2.17 | 0.00 | 1.88 | 0.27 | 0.08 | 0.91 | 0.72 | 0.00 | 2.01 | 0.75 | 0.50 | 0.53 | 7.97 | 5.30 | 6.01 |
| **9.37** | 2.08 | 0.10 | 3.08 | 0.14 | 0.06 | 0.23 | 0.87 | 0.28 | 0.62 | 0.37 | 0.45 | 0.61 | 8.03 | 5.58 | 7.64 |
| **9.47** | 2.52 | 0.11 | 3.49 | 0.08 | 0.06 | 0.26 | 1.12 | 0.61 | 0.03 | 0.36 | 0.32 | 1.36 | 8.29 | 5.79 | 11.51 |
| **9.87** | 1.95 | 0.00 | | 0.09 | 0.13 | 0.41 | 1.13 | 0.00 | 0.00 | 0.29 | 0.00 | 3.42 | 8.26 | 6.16 | 23.66 |
| **9.91** | 2.29 | 1.40 | 2.01 | 0.21 | 0.10 | 0.36 | 1.48 | 0.06 | 1.87 | 0.67 | 0.51 | 4.30 | 6.72 | 5.80 | 21.37 |
| **10.49** | 2.09 | 0.53 | 1.87 | 0.16 | 0.10 | 0.35 | 1.01 | 0.48 | 0.98 | 0.52 | 0.52 | 2.47 | 7.65 | 5.60 | 15.70 |
| **10.62** | 1.78 | 0.07 | 3.79 | 0.11 | 0.09 | 0.36 | 0.76 | 0.00 | 0.82 | 0.37 | 0.42 | 0.15 | 8.50 | 5.53 | 5.40 |
| **10.88** | 1.85 | 0.00 | 3.63 | 0.11 | 0.17 | 0.90 | 0.79 | 0.14 | 0.60 | 0.45 | 0.27 | 0.77 | 9.79 | 6.03 | 5.13 |
| **10.97** | 1.73 | 0.04 | 3.99 | 0.45 | 0.07 | 0.32 | 0.59 | 0.05 | 0.66 | 0.29 | 0.44 | 0.20 | 8.86 | 5.78 | 4.97 |
| **11.32** | 1.99 | 0.00 | 2.06 | 0.18 | 0.10 | 0.35 | 0.61 | 0.82 | 0.03 | 0.32 | 0.47 | 1.26 | 8.60 | 6.00 | 7.41 |
| **11.69** | 1.85 | 0.04 | 2.75 | 0.13 | 0.07 | 0.28 | 0.65 | 0.16 | 0.84 | 0.37 | 0.52 | 0.33 | 8.21 | 5.43 | 2.24 |
| **11.98** | 1.89 | 0.35 | 1.17 | 0.39 | 0.09 | 0.44 | 1.07 | 1.06 | 0.68 | 0.54 | 0.53 | 1.47 | 7.76 | 6.17 | 4.32 |
| **12.01** | 1.76 | 0.00 | 2.70 | 0.08 | 0.20 | 0.74 | 0.70 | 0.22 | 0.70 | 0.48 | 0.35 | 0.31 | 8.65 | 5.48 | 3.17 |
| **12.17** | 1.82 | 0.25 | 3.46 | 0.42 | 0.09 | 0.27 | 0.83 | 0.44 | 0.03 | 0.29 | 0.30 | 1.20 | 8.16 | 5.76 | 9.48 |
| **12.56** | 1.83 | 0.00 | 6.81 | 0.07 | 0.04 | 0.18 | 0.34 | 0.15 | 0.18 | 0.14 | 0.34 | 1.10 | 10.10 | 6.72 | 1.03 |
| **13.90** | 2.13 | 1.76 | 0.71 | 0.23 | 0.21 | 0.43 | 0.64 | 1.05 | 3.15 | | 0.80 | | | | |
| **14.24** | 2.02 | 0.00 | 3.64 | 0.18 | 0.08 | 0.64 | 0.61 | 0.42 | 0.14 | 0.34 | 0.27 | 0.42 | 10.00 | 6.00 | 0.53 |
| **14.85** | 2.14 | 0.01 | 4.01 | 0.10 | 0.37 | 0.42 | 0.75 | 0.45 | 0.03 | 0.36 | 0.23 | 2.35 | 8.21 | 5.90 | 15.87 |
| **15.88** | 1.95 | 0.01 | 1.11 | 0.23 | 0.08 | 0.65 | 0.86 | 0.00 | 3.06 | 0.67 | 0.63 | 3.07 | 8.77 | 7.25 | 19.56 |
| **16.07** | 2.02 | 0.00 | 2.42 | 0.22 | 0.13 | 0.57 | 0.72 | 0.46 | 0.53 | 0.39 | 0.43 | 0.32 | 9.00 | 6.18 | 12.18 |
| **16.63** | 1.73 | 0.14 | 2.03 | 0.16 | 0.05 | 0.26 | 1.02 | 0.71 | 0.06 | 0.38 | 0.38 | 0.60 | | 5.61 | 5.80 |
| **16.74** | 1.88 | 0.00 | 4.89 | 0.09 | 0.08 | 0.34 | 0.44 | 0.31 | 0.06 | 0.21 | 0.28 | 0.54 | 9.90 | 6.13 | 4.68 |
| **17.12** | 1.89 | 0.08 | 1.93 | 0.14 | 0.06 | 0.44 | 1.01 | 0.62 | 0.47 | 0.45 | 0.43 | 0.63 | | 5.82 | 8.30 |
| **17.80** | 2.11 | 0.00 | 1.39 | 0.02 | 0.01 | 0.10 | 0.00 | | 0.85 | 0.31 | 0.95 | 0.17 | | 5.91 | 2.61 |
| **17.95** | 1.83 | 0.00 | 1.46 | 0.45 | 0.06 | 0.29 | 0.79 | 1.09 | 0.00 | 0.35 | 0.50 | 0.81 | 9.58 | 6.38 | 5.11 |

TABLE 1
*(continued)*

| Depth (mbsf) | TOC wt.% | TIC wt.% | TOC / TIS | $Fe_{asc}$ wt.% | $Fe_{dith}$ wt.% | $Fe_{ox}$ wt.% | $Fe_{NaAc}$ wt.% | $Fe_{py}$ wt. % | $Fe_{AVS}$ wt. % | $Fe_{HR}$ / $Fe_T$ | $(Fe_{py}+Fe_{AVS})$ / $Fe_{HR}$ | Mn wt % | Al wt.% | $Fe_T$ wt.% | Mo ppm |
|---|---|---|---|---|---|---|---|---|---|---|---|---|---|---|---|
| **18.02** | 2.01 | 0.00 | 1.73 | 0.19 | 0.10 | 0.29 | 0.66 | 0.40 | 1.22 | 0.40 | 0.63 | 0.25 | 8.79 | 6.69 | 28.62 |
| **18.15** | 2.37 | 0.00 | 3.43 | 0.09 | 0.10 | 0.17 | 0.90 | | 1.21 | 0.43 | 0.49 | 0.91 | 7.23 | 5.69 | 11.28 |
| **18.35** | 2.01 | 0.00 | 1.27 | 0.02 | 0.02 | 0.01 | 0.05 | 1.37 | 0.03 | 0.26 | 0.94 | 0.23 | 8.04 | 5.76 | 6.37 |
| **18.76** | 1.82 | 0.03 | 2.45 | 0.22 | 0.08 | 0.30 | 0.84 | | 0.75 | 0.39 | 0.47 | 0.52 | | 5.76 | 3.01 |
| **19.31** | 1.44 | 0.01 | 0.83 | 0.03 | 0.00 | 0.11 | 0.05 | 1.50 | 0.00 | 0.27 | 0.90 | 1.22 | 9.01 | 6.11 | 8.98 |
| **19.55** | 2.60 | 0.21 | 1.61 | 0.02 | 0.05 | 0.08 | 0.00 | 0.98 | 0.86 | 0.33 | 0.96 | 0.90 | | 5.91 | 26.90 |
| **19.60** | 2.05 | 0.00 | 1.15 | 0.01 | 0.01 | 0.04 | 0.03 | 1.22 | 0.67 | 0.34 | 0.96 | 1.52 | 8.65 | 5.84 | 27.37 |
| **19.93** | 3.52 | 0.65 | 2.17 | 0.03 | 0.03 | 0.05 | 0.05 | 1.28 | 0.26 | 0.32 | 0.94 | 2.26 | | 5.23 | 63.72 |
| **20.44** | 5.83 | | 2.53 | 0.02 | 0.00 | 0.04 | 0.01 | 1.98 | 0.05 | 0.41 | 0.97 | 5.48 | | 5.11 | 27.86 |
| **20.83** | 5.38 | 0.01 | 1.60 | 0.02 | 0.03 | 0.01 | 0.15 | 2.88 | 0.09 | 0.57 | 0.93 | 3.64 | 7.20 | 5.60 | 87.75 |
| **21.20** | 4.13 | 2.04 | 1.85 | 0.03 | 0.00 | 0.04 | 0.00 | 1.63 | 0.62 | 0.52 | 0.98 | 6.89 | | 4.44 | 70.12 |
| **21.95** | 6.43 | 0.01 | 1.90 | 0.31 | 0.03 | 0.06 | 0.32 | 2.94 | 0.02 | 0.75 | 0.89 | 0.29 | 4.92 | 4.47 | 78.97 |
| **22.19** | 6.58 | 0.00 | 3.08 | 0.25 | 0.02 | 0.05 | 0.27 | | 0.49 | 0.58 | 0.87 | 2.88 | 4.46 | 4.23 | 63.09 |
| **22.25** | | 0.97 | | 0.13 | 0.04 | 0.09 | 0.79 | | 0.00 | 0.64 | 0.69 | 0.69 | 5.21 | 4.57 | 117.58 |
| **22.27** | 5.79 | 0.00 | 2.17 | 0.03 | 0.04 | 0.00 | 0.10 | | 0.01 | 0.43 | 0.93 | 2.07 | 6.47 | 5.78 | 58.57 |
| **22.32** | 4.42 | 1.79 | 3.11 | 0.01 | 0.00 | 0.03 | 0.00 | 0.95 | 0.57 | 0.33 | 0.98 | 6.24 | | 4.71 | 28.99 |
| **22.84** | 6.05 | 1.01 | 2.35 | 0.03 | 0.03 | 0.04 | 0.09 | 2.15 | 0.20 | 0.57 | 0.94 | 3.43 | | 4.37 | 71.32 |
| **23.07** | 5.35 | 0.01 | 6.39 | 0.03 | 0.02 | 0.04 | 0.10 | 0.13 | 1.20 | 0.23 | 0.88 | 4.77 | 7.76 | 6.70 | 75.57 |
| **23.36** | | | | 0.05 | 0.03 | 0.04 | 0.01 | 1.54 | 0.04 | 0.36 | 0.97 | 5.98 | | 4.56 | 58.69 |
| **23.63** | 5.15 | 0.30 | 2.00 | 0.04 | 0.01 | 0.02 | 0.07 | 2.23 | 0.03 | 0.58 | 0.96 | 1.36 | | 4.05 | 46.91 |
| **24.01** | 6.74 | 1.25 | 3.37 | 0.07 | 0.01 | 0.02 | 0.00 | 1.73 | 0.02 | 0.44 | 0.99 | 4.37 | | 4.02 | 23.74 |
| **24.50** | 4.80 | 0.01 | 2.67 | 0.13 | 0.04 | 0.10 | 0.15 | 1.55 | 0.03 | 0.48 | 0.86 | 3.92 | 4.99 | 3.91 | 62.64 |
| **24.53** | 2.67 | 1.87 | 2.02 | 0.05 | 0.00 | 0.04 | 0.10 | 1.10 | 0.11 | 0.29 | 0.90 | 5.74 | | 4.67 | 44.42 |
| **24.58** | 5.78 | 0.01 | 3.29 | 0.08 | 0.03 | 0.06 | 0.18 | 1.25 | 0.56 | 0.69 | 0.84 | 4.05 | 3.16 | 3.13 | 54.63 |
| **24.63** | 4.93 | 0.01 | 2.89 | 0.23 | 0.03 | 0.10 | 0.20 | | 0.01 | 0.32 | 0.84 | 4.46 | 8.49 | 5.66 | |
| **25.29** | | 2.71 | | 0.15 | 0.03 | 0.14 | 0.21 | | 0.00 | 0.15 | 0.31 | 0.00 | 4.25 | 3.51 | 46.53 |
| **25.42** | 3.28 | 0.04 | 4.35 | 0.10 | 0.03 | 0.13 | 0.19 | 0.35 | 0.60 | 0.40 | 0.75 | 4.31 | 5.35 | 3.30 | |
| **25.54** | 5.28 | 3.01 | 9.44 | 0.15 | 0.17 | 0.09 | 0.58 | 0.16 | 0.65 | 0.50 | 0.55 | 9.60 | | 3.30 | 41.11 |
| **25.81** | 7.66 | 0.02 | 4.16 | 0.16 | 0.22 | 0.12 | 0.32 | 1.57 | 0.07 | 0.45 | 0.79 | 0.00 | 5.41 | 5.10 | 149.67 |
| **25.94** | 2.12 | 0.01 | 1.29 | 0.05 | 0.01 | 0.13 | 0.08 | 1.44 | 0.00 | 1.00 | 0.87 | 6.66 | 2.31 | 1.50 | |
| **26.05** | 3.50 | 0.00 | 2.72 | 0.08 | 0.02 | 0.21 | 0.11 | 1.12 | 0.00 | 0.14 | 0.78 | 0.00 | 20.30 | 10.86 | 20.70 |
| **26.30** | 2.60 | 0.01 | | 0.16 | 0.02 | 0.17 | 0.39 | 0.00 | 0.00 | 0.10 | 0.00 | 0.56 | 8.14 | 5.61 | 31.12 |
| **26.66** | 3.01 | 0.00 | 2.47 | 0.09 | 0.01 | 0.18 | 0.14 | 1.05 | 0.01 | 0.25 | 0.77 | 2.27 | 9.29 | 5.63 | 4.45 |
| **26.75** | 2.33 | 0.00 | 10.44 | 0.08 | 0.05 | 0.39 | 0.44 | 0.18 | 0.02 | 0.22 | 0.18 | 0.08 | 7.92 | 5.27 | 2.62 |

TABLE 1
*(continued)*

| Depth (mbsf) | TOC wt.% | TIC wt.% | TOC TIS | $Fe_{asc}$ wt.% | $Fe_{dith}$ wt.% | $Fe_{ox}$ wt.% | $Fe_{NaAc}$ wt.% | $Fe_{py}$ wt. % | $Fe_{AVS}$ wt. % | $Fe_{HR}$ / $Fe_T$ | $(Fe_{py}+Fe_{AVS})$ / $Fe_{HR}$ | Mn wt % | Al wt.% | $Fe_T$ wt.% | Mo ppm |
|---|---|---|---|---|---|---|---|---|---|---|---|---|---|---|---|
| **26.75** | 2.66 | 0.00 | 2.03 | 0.17 | 0.07 | 0.37 | 0.29 | 1.14 | 0.00 | 0.32 | 0.63 | 0.11 | 8.63 | 5.82 | 3.51 |
| **27.90** | 1.04 | 0.00 | 24.13 | 0.09 | 0.08 | 0.50 | 0.27 | 0.04 | 0.00 | 0.19 | 0.05 | 0.07 | 9.82 | 4.62 | |
| **27.98** | 1.07 | 0.02 | 10.99 | 0.17 | 0.04 | 0.26 | 0.21 | 0.08 | 0.01 | 0.12 | 0.16 | 0.07 | | 4.93 | 0.72 |
| **28.27** | 0.87 | 0.00 | 23.97 | 0.09 | 0.06 | 0.64 | 0.33 | 0.03 | 0.01 | 0.20 | 0.04 | 0.00 | 9.41 | 5.24 | 3.09 |
| **28.47** | 1.78 | 0.00 | 12.27 | 0.04 | 0.03 | 0.42 | 0.18 | 0.12 | 0.01 | 0.13 | 0.17 | 0.30 | 9.48 | 6.02 | 7.85 |
| **31.04** | 0.45 | 0.00 | 23.08 | 0.05 | 0.04 | 0.42 | 0.32 | 0.01 | 0.01 | 0.14 | 0.03 | 0.04 | 9.47 | 6.20 | 0.45 |
| **33.01** | 0.72 | 0.00 | 71.20 | 0.03 | 0.03 | 0.33 | 0.27 | 0.01 | 0.00 | 0.12 | 0.02 | 0.03 | 8.68 | 5.52 | 0.58 |
| **34.96** | 0.52 | 0.00 | 53.69 | 0.06 | 0.04 | 0.42 | 0.22 | 0.01 | | 0.11 | 0.01 | 0.02 | 10.34 | 6.71 | 0.52 |
| **37.17** | 0.55 | 0.00 | 39.45 | 0.06 | 0.05 | 0.40 | 0.28 | 0.01 | | 0.13 | 0.02 | 0.01 | 9.96 | 6.04 | 0.96 |
| **39.25** | 0.54 | 0.00 | 163.57 | 0.07 | 0.03 | 0.00 | 0.27 | 0.00 | | 0.00 | | 0.01 | 11.62 | 6.91 | 0.61 |
| **40.73** | 0.69 | 0.00 | 48.77 | 0.07 | 0.08 | 0.66 | 0.43 | 0.01 | | 0.20 | 0.01 | 0.03 | 8.55 | 6.18 | 0.67 |
| **42.23** | 0.71 | 0.00 | 31.92 | 0.09 | 0.06 | 0.62 | 0.38 | 0.02 | | | 0.02 | | 0.00 | 0.00 | 0.48 |
| **42.25** | 0.47 | | 24.52 | | | | | 0.02 | | 0.00 | | 0.05 | 10.31 | 6.18 | |
| **43.25** | | 0.00 | | 0.10 | 0.07 | 0.62 | 0.38 | | | 0.20 | 0.00 | 0.07 | 7.62 | 5.82 | 0.97 |
| **44.55** | | 0.00 | | 0.08 | 0.06 | 0.66 | 0.33 | 0.01 | | 0.19 | 0.01 | 0.03 | 7.81 | 6.00 | 0.61 |
| **47.05** | 0.61 | 0.00 | 42.23 | 0.03 | 0.05 | 0.26 | 0.31 | 0.01 | | 0.12 | 0.02 | 0.03 | 7.86 | 5.77 | 0.73 |
| **48.35** | 0.77 | 0.00 | 63.02 | 0.04 | 0.03 | 0.50 | 0.29 | 0.01 | | 0.14 | 0.01 | 0.04 | 8.62 | 6.40 | 0.68 |
| **49.25** | 0.56 | 0.00 | 39.20 | 0.04 | 0.03 | 0.03 | 0.20 | 0.01 | | 0.04 | 0.04 | 0.05 | 12.89 | 7.97 | 0.64 |
| **49.60** | 0.55 | | 44.66 | | | | | 0.01 | | | | 0.02 | 8.70 | 5.43 | |
| **51.25** | 0.46 | 0.00 | 29.89 | 0.04 | 0.03 | 0.70 | 0.20 | 0.01 | | 0.18 | 0.01 | 0.03 | 8.01 | 5.40 | 0.76 |
| **52.60** | | 0.00 | | 0.02 | 0.03 | 0.52 | 0.13 | 0.01 | | 0.11 | 0.01 | 0.04 | 10.00 | 6.47 | 0.67 |
| **53.05** | 0.34 | 0.00 | 31.03 | 0.02 | 0.02 | 0.00 | 0.00 | 0.01 | | | | 0.02 | 8.41 | 5.94 | 0.64 |
| **54.65** | 0.49 | 0.00 | 40.90 | 0.02 | 0.02 | 0.39 | 0.09 | 0.01 | | 0.08 | 0.02 | 0.02 | 9.65 | 6.19 | 0.58 |
| **55.25** | 0.33 | 0.00 | 32.08 | 0.02 | 0.02 | 0.37 | 0.06 | 0.01 | | | 0.02 | | 0.00 | 0.00 | |
| **55.95** | | 0.00 | | 0.02 | 0.01 | 0.41 | 0.10 | 0.01 | | 0.09 | 0.02 | 0.02 | 9.76 | 6.45 | 0.50 |
| **57.25** | 0.29 | 0.00 | 24.61 | 0.02 | 0.00 | 0.29 | 0.08 | 0.01 | | 0.06 | 0.03 | 0.04 | 9.67 | 6.76 | 0.65 |
| **59.10** | 0.19 | 0.00 | 63.80 | 0.01 | 0.04 | 0.25 | 0.04 | 0.00 | | | 0.01 | 0.06 | 6.91 | 4.89 | 0.51 |
| **60.25** | 0.28 | 0.00 | 22.77 | 0.02 | 0.01 | 0.36 | 0.08 | 0.01 | | 0.07 | 0.02 | 0.05 | 9.57 | 6.56 | 0.55 |
| **61.25** | 0.46 | 0.00 | 71.16 | 0.01 | 0.09 | 0.38 | 0.05 | 0.01 | | 0.09 | 0.01 | 0.03 | 10.26 | 5.98 | 0.62 |
| **61.90** | 0.34 | 0.00 | 49.16 | 0.01 | 0.01 | 0.26 | 0.06 | 0.01 | | | 0.02 | 0.08 | 8.74 | 6.54 | 0.51 |
| **63.25** | 0.37 | 0.00 | 136.89 | 0.02 | 0.04 | 0.38 | 0.09 | 0.00 | | 0.09 | 0.00 | 0.04 | 8.26 | 5.76 | 0.63 |
| **65.15** | 0.21 | 0.00 | 8.67 | 0.01 | 0.07 | 0.36 | 0.09 | 0.02 | | 0.09 | 0.04 | 0.04 | 9.47 | 6.38 | 0.46 |
| **66.15** | 0.23 | 0.00 | 17.82 | 0.01 | 0.01 | 0.37 | 0.10 | 0.01 | | 0.09 | 0.02 | 0.04 | 9.81 | 5.90 | 0.60 |
| **67.25** | 0.32 | 0.00 | 186.80 | 0.01 | 0.07 | 0.35 | 0.10 | 0.00 | | 0.09 | 0.00 | 0.03 | 8.94 | 5.88 | 1.11 |
| **67.95** | 0.23 | 0.00 | 24.42 | 0.01 | 0.01 | 0.38 | 0.09 | 0.01 | | 0.11 | 0.02 | 0.01 | 6.42 | 4.47 | 0.45 |

TABLE 1
*(continued)*

| Depth (mbsf) | TOC wt.% | TIC wt.% | TOC / TIS | $Fe_{asc}$ wt.% | $Fe_{dith}$ wt.% | $Fe_{ox}$ wt.% | $Fe_{NaAc}$ wt.% | $Fe_{py}$ wt. % | $Fe_{AVS}$ wt. % | $Fe_{HR}$ / $Fe_T$ | $(Fe_{py}+Fe_{AVS})$ / $Fe_{HR}$ | Mn wt % | Al wt.% | $Fe_T$ wt.% | Mo ppm |
|---|---|---|---|---|---|---|---|---|---|---|---|---|---|---|---|
| **69.25** | 0.27 | 0.00 | 23.50 | 0.01 | 0.08 | 0.35 | 0.07 | 0.01 | | 0.12 | 0.02 | 0.02 | 7.26 | 4.23 | 0.55 |
| **71.15** | 0.23 | | 12.60 | 0.01 | 0.03 | 0.38 | 0.07 | 0.02 | | | 0.03 | | | 0.00 | |
| **72.15** | 0.17 | 0.00 | 14.00 | 0.01 | 0.01 | 0.28 | 0.08 | 0.01 | | 0.09 | 0.03 | 0.02 | 8.11 | 4.45 | 0.47 |
| **73.25** | 0.16 | 0.00 | 146.23 | 0.01 | 0.04 | 0.21 | 0.08 | 0.00 | | 0.06 | 0.00 | 0.03 | 9.15 | 5.68 | 0.99 |
| **76.55** | 0.20 | 0.00 | 9.81 | 0.01 | 0.03 | 0.41 | 0.04 | 0.02 | | 0.10 | 0.03 | 0.03 | 9.60 | 5.08 | 0.62 |
| **79.75** | 0.12 | 0.00 | 14.81 | 0.01 | 0.02 | 0.26 | 0.05 | 0.01 | | 0.09 | 0.02 | 0.02 | 6.54 | 3.68 | 0.08 |
| **83.05** | 0.14 | 0.00 | 6.11 | 0.01 | 0.03 | 0.28 | 0.04 | 0.02 | | | 0.05 | 0.07 | 8.01 | 5.20 | 0.56 |
| **86.35** | 0.17 | 0.00 | 6.44 | 0.00 | 0.02 | 0.28 | 0.04 | 0.02 | | 0.10 | 0.06 | 0.02 | 7.09 | 3.59 | 0.52 |
| **89.65** | 0.20 | 0.00 | 6.63 | 0.00 | 0.03 | 0.19 | 0.04 | 0.03 | | 0.12 | 0.09 | 0.00 | 6.72 | 2.32 | 0.51 |

standard NOD-1 yielded an average $\delta^{98}$Mo value of −0.29 permil and 1σ of 0.04 permil, similar to previously reported values (Asael and others, 2013). Values for Mo isotope measurements and associated error can be found in table 2. We analyzed duplicates or more from 48 individual samples, resulting in $1\sigma < 0.11$ permil and mostly <0.06 permil.

## RESULTS

### *Carbon and Sulfur*

Starting near ~26.75 mbsf, TOC concentrations increase up section from <0.5 weight percent to >2 weight percent (fig. 2A). This switch in TOC occurs in concert with an increase in diatom abundance inferred to record the transition from the Ancylus Lake into the Littorina Sea (Andrén and others, 2015). There are two peaks in TOC above ~26.75 mbsf that indicate two sapropels at ~19.5 to 26.75 mbsf and ~4.3 to 7.3 mbsf, with maxima between 7 to 8 weight percent. Peaks in TIC abundance also occur within these sapropels. A similar trend to that of TOC is observed for total inorganic sulfur (TIS), which represents the sum of sulfur from the AVS and CRS extractions (fig. 2B). C/S ratios were calculated using the ratio of TOC to TIS (fig. 2C).

### *Iron and Manganese*

As products of glacial runoff in an oxic setting, $Fe_T/Al$ and $Fe_{HR}/Fe_T$ from the Baltic glacial lake clays below 26.75 mbsf provide an integrated detrital sediment record for the catchment area (Goldschmidt, 1933) (fig. 3A). Though Baltic detrial $Fe_T/Al$ values have previously been reported as 0.6 to 0.65 (Fehr and others, 2008), to be conservative we will interpret anoxia from $Fe_T/Al$ ratios above the highest value from the ice lake sediments, which is 0.75 (vertical dashed line fig. 3A). Importantly, a baseline of 0.65 is consistent with most of our samples and if applied would have little impact on our final interpretations. For $Fe_{HR}/Fe_T$ ratios ($Fe_{HR}$ defined here as the sum of $Fe_{AVS}$, $Fe_{CRS}$, $Fe_{ox}$, $Fe_{NaAc}$, $Fe_{asc}$, and $Fe_{dith}$), we identify the presence of past water column anoxia using a threshold value of 0.38 as previously determined (Raiswell and Canfield, 1998) and commonly applied in the literature (Poulton and Canfield, 2011)—and consistent with the Landsort Deep lacustrine sediments below 26.75 mbsf.

Starting near the lacustrine-brackish boundary at ~26.75 mbsf and moving up section, there is a distinct increase in $Fe_T/Al$ and $Fe_{HR}/Fe_T$ ratios above the detrital background, with large peaks in close association with the sapropel units and some outside of sapropel deposition, and in association with peaks in Mo concentration (fig. 3; fig. 4; figs. 5A and 5B). The $Fe_T/Al$ values approach 1 in the lower sapropel and 1.4 in the upper sapropel, both of which are well above the detrital baseline. Between 7.4 to 3.4 mbsf, there are cases where $Fe_{HR}$ exceeds $Fe_T$, in which case $Fe_{HR}/Fe_T$ is plotted as 1. This artifact may reflect sample heterogeneity, as sample splits for individual analyses come from unhomogenized bulk samples.

For intervals with elevated $Fe_{HR}/Fe_T$ and $Fe_T/Al$, we use $(Fe_{py} + Fe_{AVS})/Fe_{HR}$ values of >0.6 as the threshold for delineating past euxinia. Supporting this choice, a crossplot of $(Fe_{py} + Fe_{AVS})/Fe_{HR}$ versus Mo (not shown) indicates that Mo concentrations >25 ppm, which are typical of euxinic deposition (Scott and Lyons, 2012), are nearly exclusively associated with $(Fe_{py} + Fe_{AVS})/Fe_{HR}$ values >0.6. Alternatively, Mo concentrations >10 ppm could indicate short-lived/intermittent or weakly euxinic episodes, which may be supported by coupled increases in Mo >10 ppm in association with elevated $Fe_{HR}/Fe_T$ and $Fe_T/Al$, which are noted in figure 3D. However, our approach of a euxinic/ferruginous $(Fe_{py} + Fe_{AVS})/Fe_{HR}$ threshold of ~0.6 is conservative in that it minimizes the likelihood of false ferruginous interpretations. We also note that the $Fe_{asc}$ and $Fe_{dith}$ data from the samples collected onshore indicate that some post-drilling oxidation of Fe-sulfides has occurred, and thus $Fe_{asc}$ and $Fe_{dith}$ are

TABLE 2

*Mo isotope data*

| Sample Depth (mbsf) | $\delta^{98/95}$Mo (‰) | 1s | Sample Depth (mbsf) | $\delta^{98/95}$Mo (‰) | 1s |
|---|---|---|---|---|---|
| 0.70 | -0.28 | 0.03 | 9.47 | -0.05 | 0.02 |
| 0.70 | -0.25 | 0.04 | 9.91 | -0.37 | 0.03 |
| 0.70 | -0.24 | 0.03 | 9.91 | -0.39 | 0.03 |
| 1.47 | -0.46 | 0.03 | 10.49 | -0.38 | 0.03 |
| 1.47 | -0.49 | 0.03 | 10.49 | -0.36 | 0.03 |
| 2.04 | -0.02 | 0.03 | 11.69 | -0.16 | 0.03 |
| 2.04 | 0.06 | 0.04 | 11.69 | -0.04 | 0.03 |
| 2.56 | 0.19 | 0.03 | 14.24 | -0.47 | 0.03 |
| 2.56 | 0.08 | 0.02 | 14.24 | -0.43 | 0.03 |
| 2.97 | 0.18 | 0.03 | 14.24 | -0.41 | 0.03 |
| 2.97 | 0.18 | 0.02 | 14.24 | -0.48 | 0.04 |
| 3.34 | 0.06 | 0.03 | 14.24 | -0.49 | 0.05 |
| 3.34 | 0.03 | 0.03 | 14.24 | -0.51 | 0.03 |
| 3.55 | -0.13 | 0.03 | 14.24 | -0.44 | 0.02 |
| 3.55 | -0.11 | 0.03 | 16.07 | -0.11 | 0.03 |
| 3.99 | 0.19 | 0.03 | 16.07 | -0.10 | 0.03 |
| 4.30 | -0.04 | 0.04 | 16.74 | -0.05 | 0.04 |
| 4.30 | -0.07 | 0.02 | 16.74 | -0.08 | 0.03 |
| 4.62 | 1.19 | 0.03 | 17.8 | 0.34 | 0.03 |
| 4.62 | 1.11 | 0.03 | 17.8 | 0.29 | 0.03 |
| 4.62 | 1.00 | 0.03 | 18.02 | 0.07 | 0.02 |
| 4.62 | 1.17 | 0.05 | 18.02 | 0.09 | 0.03 |
| 4.85 | -0.13 | 0.03 | 18.76 | 0.15 | 0.03 |
| 4.85 | -0.19 | 0.03 | 18.76 | 0.03 | 0.03 |
| 5.15 | -0.09 | 0.03 | 19.31 | 0.16 | 0.03 |
| 5.15 | -0.11 | 0.03 | 19.31 | 0.10 | 0.03 |
| 5.41 | -0.38 | 0.05 | 19.31 | 0.17 | 0.03 |
| 5.41 | -0.49 | 0.05 | 19.545 | -0.02 | 0.02 |
| 5.41 | -0.32 | 0.03 | 19.545 | 0.06 | 0.03 |
| 5.41 | -0.32 | 0.02 | 19.60 | 0.12 | 0.03 |
| 5.67 | -0.13 | 0.04 | 19.60 | 0.14 | 0.03 |
| 6.05 | -0.17 | 0.03 | 19.60 | 0.11 | 0.04 |
| 6.05 | -0.19 | 0.03 | 19.925 | 0.04 | 0.04 |
| 6.13 | -0.14 | 0.03 | 19.925 | 0.07 | 0.03 |
| 6.23 | -0.45 | 0.04 | 20.44 | 0.28 | 0.03 |
| 6.23 | -0.24 | 0.02 | 20.44 | 0.28 | 0.03 |
| 6.23 | -0.27 | 0.02 | 20.44 | 0.27 | 0.03 |
| 6.8 | -0.50 | 0.03 | 20.83 | 0.41 | 0.03 |
| 6.8 | -0.43 | 0.03 | 20.83 | 0.38 | 0.03 |
| 7.34 | -0.25 | 0.05 | 21.2 | 0.17 | 0.03 |
| 7.34 | -0.25 | 0.04 | 21.95 | 0.46 | 0.03 |
| 8.03 | -0.12 | 0.03 | 21.95 | 0.50 | 0.03 |
| 8.03 | -0.28 | 0.04 | 22.19 | 0.59 | 0.03 |
| 8.13 | 0.11 | 0.03 | 22.19 | 0.59 | 0.03 |
| 8.13 | 0.14 | 0.03 | 22.25 | 0.47 | 0.03 |
| 8.48 | 0.07 | 0.03 | 22.25 | 0.47 | 0.03 |
| 9.47 | -0.03 | 0.03 | 22.32 | 0.23 | 0.03 |

Table 2
*(continued)*

| Sample Depth (mbsf) | $\delta^{98/95}$Mo (‰) | 1s |
|---|---|---|
| 22.32 | 0.20 | 0.02 |
| 22.32 | 0.21 | 0.03 |
| 22.84 | 0.43 | 0.03 |
| 22.84 | 0.43 | 0.03 |
| 22.84 | 0.41 | 0.03 |
| 23.07 | 0.22 | 0.03 |
| 23.07 | 0.22 | 0.03 |
| 23.36 | 0.26 | 0.02 |
| 23.36 | 0.30 | 0.03 |
| 23.36 | 0.23 | 0.03 |
| 23.63 | 0.69 | 0.03 |
| 23.63 | 0.62 | 0.03 |
| 23.63 | 0.46 | 0.03 |
| 23.63 | 0.57 | 0.07 |
| 24.01 | 0.30 | 0.03 |
| 24.01 | 0.25 | 0.03 |
| 24.01 | 0.24 | 0.03 |
| 24.53 | 0.13 | 0.03 |
| 24.53 | 0.10 | 0.03 |
| 25.29 | 0.21 | 0.03 |
| 25.29 | 0.23 | 0.03 |
| 25.54 | 0.43 | 0.02 |
| 25.54 | 0.44 | 0.03 |
| 25.81 | 0.59 | 0.03 |
| 25.81 | 0.59 | 0.03 |
| 25.81 | 0.11 | 0.06 |
| | | |
| Sample | | |
| NOD-A-1 | -0.25 | 0.05 |
| NOD-A-1 | -0.33 | 0.04 |
| NOD-A-1 | -0.24 | 0.04 |
| NOD-A-1 | -0.33 | 0.04 |
| NOD-A-1 | -0.28 | 0.03 |
| Average | -0.29 | 0.04 |
| Standard Deviation | 0.04 | |

External precision 1STD on δ98Mo = 0.04‰.

not included in the $Fe_{HR}$ pool for calculations of $(Fe_{py} + Fe_{AVS})/Fe_{HR}$ for the onshore sample set. This omission also minimizes the likelihood of spurious ferruginous signals. However, comparison with offshore $(Fe_{py} + F_{AVS})/Fe_{HR}$ ratios that include $Fe_{dith}$ and $Fe_{asc}$ suggests little difference (green vs black points fig. 3C).

In the brackish sediments, Mn enrichments also mirror the sapropels, with values of up to 15 weight percent in the upper sapropel and near 7 weight percent in the lower sapropel (fig. 5C). These concentrations are four orders of magnitude higher than the estimated global crustal average of 0.085 weight percent (Turekian and Wedepohl, 1961) and up to five orders of magnitude above those observed for the underlying Baltic lacustrine sediments. This comparison indicates that the Baltic Mn enrichments are not a result of detrital input but instead reflect intensive Mn redox cycling persistent throughout brackish deposition.

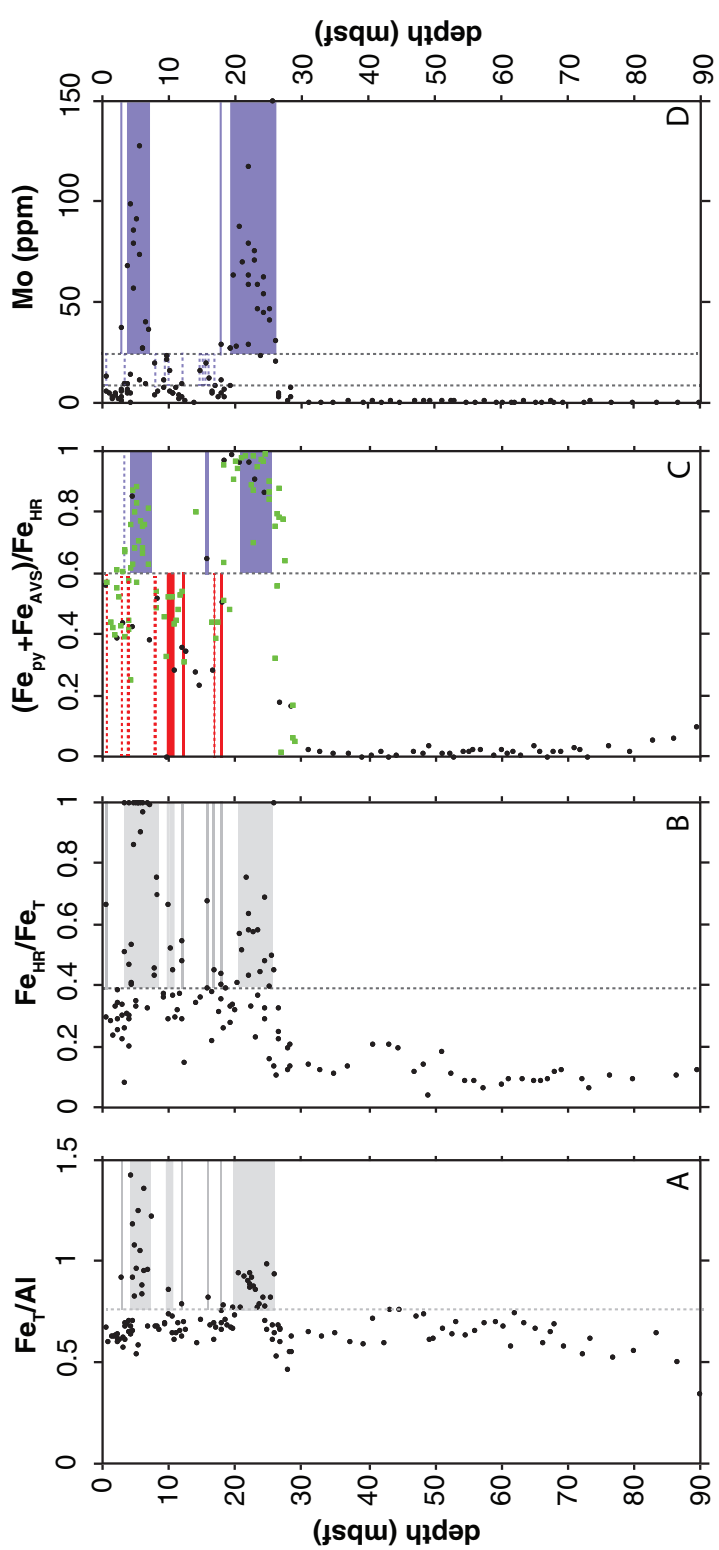


Fig. 3. M0063 down core profiles displaying: (A) Total Fe-to-Al ratios ($Fe_T/Al$), with dashed line representing our locally established Landsort Deep $Fe_T/Al$ detrital baseline of 0.75 determined from the ice lake sediments; (B) 'Highly reactive' Fe-to-total Fe ratios ($Fe_{HR}/FeT$), with vertical dashed line representing the previously established anoxic baseline of 0.38 (Raiswell and Canfield, 1998); (C) The sum of CRS-derived Fe and AVS-derived Fe-to-'highly reactive' Fe ($(Fe_{py} + Fe_{AVS})/Fe_{HR}$), with vertical dashed line representing the ferruginous-euxinic baseline of 0.6 determined specifically for this study. Green squares indicate samples collected onshore where $Fe_{HR}$ does not include $Fe_{dith}$ and $Fe_{asc}$ due to indications of post-drilling Fe-sulfide oxidation; (D) Mo concentrations. The colored boxes/lines indicate specific water column redox conditions inferred from the data as, anoxic (gray), ferruginous (red), and euxinic (purple). Dashed lines in (C) represent intervals not inferred as anoxic from both $Fe_T/Al$ and $Fe_{HR}/Fe_T$ and dashed lines in (D) represent possible euxinic conditions indicated by 10-25 ppm Mo, which together overlap with each of the increases in $Fe_T/Al$ or $Fe_{HR}/Fe_T$ above detrital baselines.

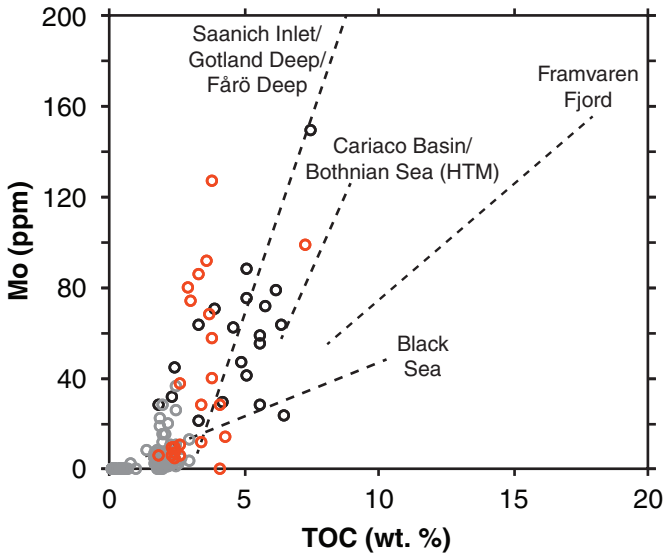


Fig. 4. Crossplot of Mo concentration against total organic carbon (TOC). Colors correspond to the upper (red) and lower sapropels (black) and all other intervals (gray). Dashed lines represent Mo vs TOC slopes for other modern and past euxinic basins as determined in previous studies (Algeo and Lyons, 2006; Jilbert and Slomp, 2013; Jilbert and others, 2015). The line for the Bothnian Sea refers specifically to the Holocene Thermal Maximum or HTM (Jilbert and others, 2015). Sapropel intervals correspond to that of figure 2.

### *Molybdenum*

Molybdenum concentrations rise above 1 ppm at the transition from lacustrine to brackish sedimentation in the Landsort Deep, reaching values >100 ppm in the intervals associated with sapropel deposition from ~19.5 to 26.3 mbsf and 4.30 to 7.34 mbsf (fig. 3D, fig. 4, fig. 5B). For Mo isotopes, we performed 123 individual measurements for 52 samples. Our results show that, although sedimentary Mo is in general a mixture of detrital and authigenic sources, the Mo in the lacustrine interval is mainly of detrital origin as indicated by the Mo concentrations of <1 ppm, which are typical of average continental crust. Therefore, no Mo isotope measurements were performed for the lacustrine sediments. The $\delta^{98}$Mo have a total range of −0.5 to +1.11 permil (fig. 5D). From ~20 to 26 mbsf, overlapping with the lower sapropel, $\delta^{98}$Mo values are variable within a distinct range of +0.10 to +0.62 permil relative to the remainder of the profile. Starting at 20 mbsf, there is an upward shift to more negative values, with a range of −0.50 to +0.29 permil and one outlier of 1.11 permil at 4.62 mbsf. From ~4.8 to 8 mbsf, overlapping with the upper sapropel, $\delta^{98}$Mo values show a distinctly negative range of −0.50 to −0.11 permil.

### *Pore Waters*

Interstitial waters were analyzed as part of the IODP Expedition 347 and are described in detail in the expedition report (Andrén and others, 2015). We use these interstitial water data to complement our corresponding sedimentary data and for the calculation of saturation indices, particularly for rhodochrosite. Briefly, pore water Mn concentrations increase moving upward in the profile to a peak value of ~1.5 mM (fig. 6B). Pore water alkalinity shows a broad peak in association with the brackish sediments, with a peak value of ~58 meq/L at ~14.5 mbsf (fig. 6B).

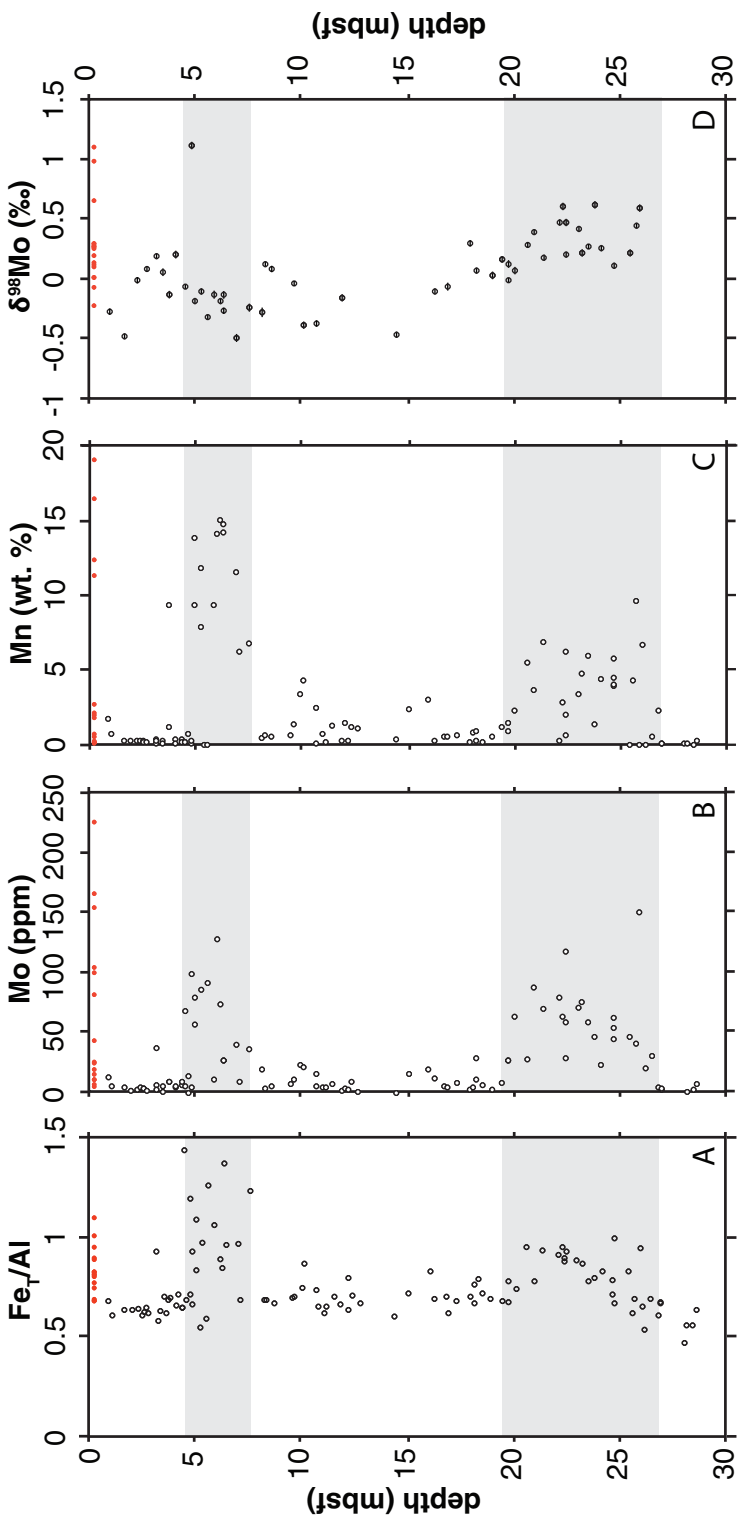


Fig. 5. M0063 down core profiles showing the upper 30 mbsf for (A) $Fe_T$/Al from figures 3A and 3B. Mo concentrations from figures 3D and 3C. Mn concentrations; (D) Mo isotope values ($\delta^{98}$Mo). Error bars are shown in part D, but are typically smaller than the data points. Red dots at the top of each panel show data from Noordman and others (2015) for the upper 15 cm of Landsort Deep, representing the modern-recent euxinic period not captured in this study. The shaded gray areas indicate the sapropels from 26.75 to 19.5, and 7.3 to 4.3 mbsf, as indicated from TOC in figure 2.

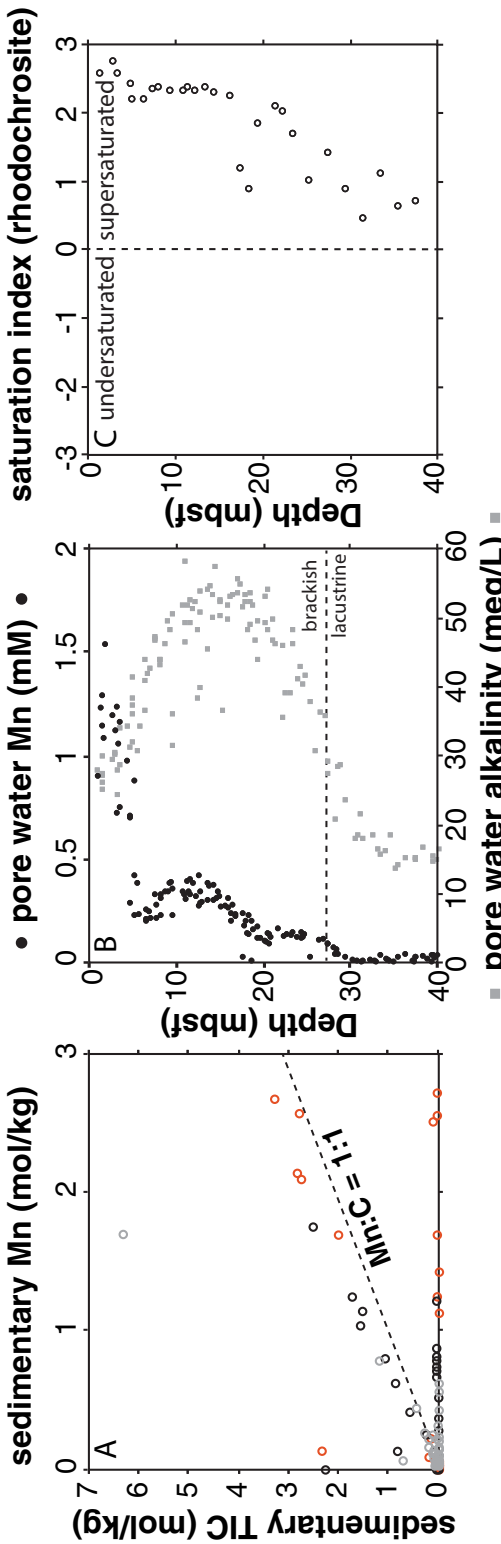


Fig. 6. (A) Crossplot of total inorganic carbon (TIC) and Mn concentrations. As in figure 4, the colors correspond the lower sapropel (black), upper sapropel (red), and all other intervals (gray), with sapropel intervals corresponding to that of figure 2A. The dashed line represents the relationship expected for rhodochrosite assuming a chemical formula of $MnCO_3$. (B) Pore water Mn (black circles) and alkalinity (gray squares) concentrations for the upper 40 mbsf from all holes at site M0063 (Andrén and others, 2015). Dashed line represents the lacustrine-brackish boundary, as depicted in figure 2 and described in the text. (C) Saturation indices for rhodochrosite calculated using PHREEQC (Parkhurst and Appelo, 1999) and using pore water data from Hole C at site M0063 (Andrén and others, 2015).

## DISCUSSION

### *Salinity Variations*

The diatom and sedimentological records from Landsort Deep, as described in detail in the IODP report for Site M0063 of Expedition 347 (Andrén and others, 2015), indicate a fresh-to-weakly brackish transition at 43 mbsf (Baltic Ice Lake-to-Yoldia Sea), a switch from brackish to fresh conditions at 41 mbsf (Yoldia Sea-to-Ancylus Lake), and a fresh-to-brackish shift near 26.75 mbsf (Ancylus Lake to Littorina Sea). Ratios of total organic carbon to total inorganic sulfur (C/S) can provide an independent indicator of salinity transitions because sulfate is typically the main factor limiting pyrite formation in freshwater lacustrine settings (Berner and Raiswell, 1983). This assumption holds true only for sediments with TOC values of >1 weight percent. At lower TOC values, organic matter may be the limiting factor, thus complicating the distinction between marine and non-marine deposition (Berner and Raiswell, 1983). Our results show a switch to TOC values of >1 weight percent at ~26.75 mbsf; below this concentration detailed fluctuations in C/S cannot be used to track salinity fluctuations (fig. 2). A general change from C/S ratios of >10 to values <5 at ~26.75 mbsf, however, is consistent with sedimentological and paleontological evidence for a switch from lacustrine to brackish deposition—marking a transition to a high TOC sapropel. In general, C/S ratios for sediments above 26.75 mbsf are <5 and specifically near the 2.8±0.8 value typical for normal (oxic) marine deposition (Berner, 1982). The shift in C/S is interpreted to capture the transition from the Ancylus Lake to Littorina Sea, occurring at ~8.5 kyrs B.P. (Andrén and others, 2011). The Yoldia Sea record of brackish deposition (<350 years) at ~ 41 to 43 mbsf, as inferred from brackish diatom abundance (Andrén and others, 2015), is not seen in our C-S geochemical proxy—reflecting poor sample resolution (n = 2) and/or limiting sulfate and organic matter.

### *Anoxic Indicators*

In this discussion and those that follow, we explore the use of geochemical proxies as tracers of past oxygen-deficiency and, in that discussion, open the door to the possibility that multiple geochemical tracers might collectively speak more convincingly to temporal stability of such conditions and the related controlling factors.

*Iron and molybdenum proxies.*—The persistence of laminations indicates likely sustained water column anoxia throughout deposition of the Baltic brackish phase. Furthermore, $Fe_T/Al$ and $Fe_{HR}/Fe_T$ ratios provide evidence for anoxic deposition for the two sapropels, as well as multiple, likely short-lived, redox oscillations outside of the sapropel deposition (figs. 3 and 5). Adding to this framework, $(Fe_{py} + Fe_{AVS})/Fe_{HR}$ and Mo concentrations suggest euxinia during sapropel deposition and multiple euxinic and potential ferruginous candidates in the surrounding brackish intervals (figs. 3 and 5). The combination of $Fe_{HR}/Fe_T$ >0.38 and Mo concentrations approaching or exceeding 100 ppm constrains euxinia for the two sapropels as being the predominant condition and thus likely occurring beyond seasonal timescales (Raiswell and Canfield, 1998; Scott and Lyons, 2012). Two distinct sapropels with inferred anoxic water column conditions have been recognized previously in the Landsort Deep past (Lepland and Stevens, 1998), and past water column euxinia has more specifically been inferred for periods throughout the Holocene at other Baltic subbasins (Boesen and Postma, 1988; Sternbeck and Sohlenius, 1997; Sternbeck and others, 2000; Sohlenius and others, 2001; Fehr and others, 2008; Jilbert and Slomp, 2013; Lenz and others, 2015). These intervals overlap roughly with the Holocene Thermal Maximum (HTM) from ~9-5 kyrs B.P. and the Medieval Climate Anomaly (MCA) from *ca.* 1.25 to 0.80 kyrs. B.P. (Zillén and others, 2008). The presence of laminations in intervals lacking geochemical indications of anoxia likely reflect the persistence of local water column redox conditions not reducing enough to support

dissolved iron or sulfide accumulation—but instead low oxygen or even anoxia that could not support benthic habitation (Dashtgard and MacEachern, 2016). Alternatively, ferruginous conditions may have prevailed during these periods, which have been shown in the modern Peruvian oxygen minimum zone to not support enhanced 'highly reactive' iron deposition in the absence of a ferruginous-oxic transition (Scholz and others, 2014).

Crossplots of Mo versus TOC can speak to the relative basin-wide extent of euxinic seafloor under different redox regimes in the Baltic by revealing the impact of the water column Mo reservoir size on local sedimentary Mo enrichments (Algeo and Lyons, 2006). The relationship of Mo versus TOC in our samples from the two Landsort Deep sapropels are similar, and both data sets are consistent with those from other euxinic sub-basins of the Baltic Proper—past and present (fig. 4) (Jilbert and Slomp, 2013). Furthermore, our results from Landsort Deep show a Mo-TOC relationship similar to that seen in the intermittently restricted Saanich Inlet, and our high Mo concentrations and Mo-TOC are easily distinguished from those of more restricted modern euxinic basins (fig. 4) (Algeo and Lyons, 2006). During exposure to sulfide, dissolved water column molybdate is progressively converted to tetrathiomolybdate (Erickson and Helz, 2000). Near-complete tetrathiomolybdate formation from molybdate occurs when water column total dissolved sulfide is stable at concentrations >100 μM (Erickson and Helz, 2000). Subsequent efficient scavenging under restricted conditions can draw down the water column Mo reservoir when renewal rates are low relative to burial. Such efficient Mo uptake can result in markedly low sedimentary Mo concentrations despite elevated TOC and independent indications for euxinia based on Fe geochemistry (Algeo and Lyons, 2006). Figure 4 shows examples of modern basins with progressively more restricted conditions with respect to Mo: Baltic Sea, Saanich Inlet < Cariaco Basin < Framvaren Fjord < Black Sea (Algeo and Lyons, 2006; Jilbert and Slomp, 2013). Intriguingly, a different Mo-TOC trend than that of the Holocene Baltic Proper is observed in the more northern Bothnian Sea (fig. 4)—specifically in association with the HTM (Jilbert and others, 2015). During this time, Bothnian sediments contain Mo enrichments indicative of euxinia and a Mo-TOC relationship more similar to the modern Cariaco Basin. Considering that the Bothnian Sea is oxic today, local evidence for stable euxinia extended beyond the Baltic Proper suggests the likelihood of more expansive euxinia in the Baltic generally during the HTM relative to today. Ultimately, however, relatively high Mo/TOC ratios in the Landsort Deep and the Baltic Proper generally indicate a high rate of Mo supply compared to the burial sink throughout the Holocene regardless of relative changes in the extent of seafloor euxinia in the Baltic generally—consistent with strong seawater exchange and a relatively small fraction of seafloor characterized by euxinia ( Jilbert and Slomp, 2013; Jilbert and others, 2015).

Interestingly, the intervals with clearly elevated $Fe_T/Al$ and $Fe_{HR}/Fe_T$ ratios have $(Fe_{py} + Fe_{AVS})/Fe_{HR}$ and Mo concentration typical of euxinia but show a range of magnitudes in $Fe_T/Al$, suggesting controls on Fe deposition in addition to the persistence of euxinic water column conditions. Multiple factors can influence primary differences in $Fe_T/Al$ and $Fe_{HR}/Fe_T$ ratios among or within basins. Importantly, the observed $Fe_T/Al$ peaks of 1.4 and 0.95 within the two Landsort Deep sapropels (fig. 4) are high compared to other modern euxinic basins (Lyons and Severmann, 2006) but are comparable to the modern Landsort Deep sediments with values as high as 1 (Noordmann and others, 2015). The diagnostic Fe enrichments are largely controlled by the rate at which Fe is transported from source regions, such as oxygen-poor sediments and bottom waters that are reducing but not sulfidic, to regions such as the Landsort Deep that are euxinic (for example, Lyons and Severmann, 2006). In these euxinic settings, the 'shuttled' Fe is captured in the water column through syngenetic

pyrite formation. If we consider the small area of the Landsort deep relative to the surrounding potential source region, the large source-to-sink ratio is expected to favor high $Fe_T/Al$ and $Fe_{HR}/Fe_T$ ratios in both sapropel intervals (Raiswell and Anderson, 2005; Lenz and others, 2015). In this view, relative to conditions during deposition of the upper sapropel, the lower $Fe_T/Al$ ratios of the lower sapropel may reflect more widespread euxinic conditions in the Landsort Deep (providing a larger Fe sink relative to the source area) or an expansion of sulfidic pore fluids and water columns in the Baltic more generally (thus decreasing the Fe source area to Landsort Deep)—or both. This interpretation is supported by detailed analyses of $Fe_T/Al$ ratios along shelf-to-basin transects that capture past euxinic regimes at the nearby Gotland Deep. In this case, maximum $Fe_T/Al$ ratios do not correspond to the time of most expansive bottom water euxinia—but instead record the initial onset and expansion of euxinia (Lenz and others, 2015). Together, the $Fe_T/Al$ and Mo-TOC relationship indicate that the extent of euxinia at Landsort Deep and likely the Baltic in general varied between deposition of the two sapropels, but the concentrations and timescales of water column sulfide accumulation euxinia consistently remained below distributions that would have significantly drawn down the Baltic Mo reservoir.

### *Stability of Reducing Conditions*

Given that our $Fe_T/Al$ results suggest potential differences between the past euxinic episodes represented by the sapropels in Landsort Deep, we apply a combination of Mn concentration and Mo isotope data to evaluate the relative stabilities and magnitudes of water-column total dissolved sulfide concentrations as recorded in these two intervals.

*Manganese concentrations.*—Our measured bulk sedimentary Mn concentrations associated with sapropel deposition, up to 7 and 15 weight percent, are extreme in a global context but are comparable to observations in the modern Baltic; Mn concentrations in sediments from the modern Landsort and Gotland Deeps range up to 10 to 18 weight percent (Sternbeck and Sohlenius, 1997; Lepland and Stevens, 1998; Noordmann and others, 2015) and even as high as 25 weight percent (Lenz and others, 2014). We suggest, as others have for Mn enrichments in modern Landsort Deep sediments (Scholz and others, 2013; Lenz and others, 2014), that the extreme enrichments observed during brackish deposition generally, but for the euxinic sapropels in particular, fingerprint oscillations between oxic and anoxic conditions in a system that was dominantly euxinic (Lepland and Stevens, 1998). As was argued in that past work, we attribute these oscillations to major Baltic inflow (MBIs) events characterized by oxygenated marine waters from the North Sea. As Mn concentrations are twice as high in the upper sapropel compared to lower, this interpretation would require relatively less stable redox conditions during upper sapropel deposition. MBIs are barotrophic events during which saline and oxygenated water from the North Sea enters the Baltic beneath the halocline (Mohrholz and others, 2015). A record of MBIs over the last century indicates that the area of Baltic seafloor anoxia decreases during such events due to replacement of previously anoxic bottom waters with oxygenated North Sea water, but anoxia resumes soon afterward due to an associated strengthening of the halocline from the input of relatively higher salinity waters from the marine North Sea compared to the brackish Baltic Sea (Carstensen and others, 2014).

Sedimentary Mn enrichments are linked to MBIs through oxidation of dissolved $Mn^{2+}$ within the anoxic Landsort Deep waters and associated deposition in the sediments as oxide mineral phases (Scholz and others, 2013; Lenz and others, 2014; Lenz and others, 2015). During burial, the oxides are re-reduced and accumulate in pore waters as dissolved $Mn^{2+}$ or, in the presence of pore water sulfide or appreciable alkalinity, precipitate as sulfide or carbonate minerals such as hauerite or rhodochrosite (Berner, 1984; Sternbeck and Sohlenius, 1997; Lepland and Stevens, 1998).

Indeed, a link is observed in our samples between total inorganic carbon (TIC) and Mn that falls along a slope similar to that for stoichiometric $MnCO_3$ (fig. 6A), suggesting the formation of Mn carbonate is a relevant Mn sink in our sediments. Importantly, however, our interpretation of MBI-associated redox oscillations from the enhanced Mn concentrations generally requires the delivery of Mn oxides to the sediments with subsequent conversion to Mn carbonate in anoxic pore waters rather than direct carbonate precipitation in the water column.

In order to establish that the source for Mn for carbonate precipitation originated from the pore waters rather than the water column, we calculated saturation indices for rhodochrosite using measured pore water $Mn^{2+}$ and alkalinity profiles from our IODP Expedition 347 sediments from M0063 collected in the Landsort Deep (Andrén and others, 2015) (figs. 6B and 6C). The pore waters host intensive dissolved $Mn^{2+}$ enrichments, up to 1.5 mM at the top of the profile (fig. 6B), providing evidence for dissolution of Mn oxides as a source of dissolved $Mn^{2+}$ to the pore fluids. Calculated using PHREEQC (Parkhurst and Appelo, 1999) and the MINTEQ databases, saturation indices indicate that rhodochrosite is supersaturated in pore waters spanning the brackish interval and extending into the lacustrine sediments (fig. 6C). These calculations favor the deposition, burial, dissolution, and diffusion of Mn that was originally associated with oxides but was subsequently reprecipitated in carbonate phases. A diagenetic origin for the Mn carbonate is generally supported by similar calculations from pore waters in modern Landsort Deep sediments (Lenz and others, 2014) and previous work that measured carbon isotope values for Mn carbonate from Landsort Deep (Suess, 1979). These efforts revealed carbonate carbon isotope values as low as −13 permil, requiring a mix of seawater and organic matter remineralization as a carbonate source.

Lastly, we point out that the extreme enrichments in Mn, interpreted to represent redox oscillations, are most prominent in association with Fe and Mo indications of the most strongly reducing conditions (fig. 6). This seemingly counterintuitive observation is partially linked to anoxic/euxinic conditions allowing for enhanced water column Mn accumulation. Given the requirement for redox oscillations for enhanced Mn burial, however, we suggest that the frequency/stamina of MBIs is also a major factor. It is well known from observations of the current anoxic period over the last century that, while the MBIs punctuate anoxia, they also provide the input of saline waters from the North Sea to the brackish Baltic. This seawater is essential for maintaining the halocline that facilitates anoxia through stronger vertical stratification (Carstensen and others, 2014). In other words, these MBIs limit the maximum reducing potential by providing oxygen-rich North Sea waters and simultaneously sustain longer-term anoxia through the introduction of seawater to Baltic bottom waters. As a proof of concept, a prolonged period lacking MBIs from 1982–1993 was marked by a decrease in the strength of Baltic haloclines in individual sub-basins as well as a decrease in the area of low oxygen bottom waters throughout the Baltic Sea, including the Landsort Deep (Carstensen and others, 2014). The frequency of these events also controls the delivery of Mn oxides to the sediments and simultaneously renews molybdate supplies to the water column, consistent with our Mo-TOC relationships suggesting an ample Mo supply to the basin. The role of MBIs as both instigators of short-term redox oscillations and as a requirement for sustained long-term anoxia again separates the Baltic from more stably reducing settings, suggesting that strongly stable euxinia throughout the Baltic is unlikely in the past—and in the future.

*Mo isotopes.*—Our Mo isotope results offer an independent constraint on redox stability, while also providing constraints on the concentrations of water column total dissolved sulfide during sapropel deposition. Our sedimentary Mo isotope data range from −0.50 to +1.11 permil, which is highly fractionated from the +2.24 to +2.67

permil values of modern Baltic seawater and similar to the −0.24 to +1.12 permil values seen in Landsort Deep sediments from the modern euxinic era (Neubert and others, 2008; Nägler and others, 2011; Noordmann and others, 2015). Two known processes allow for such large negative $\delta^{98}$Mo fractionations: euxinic conditions with water column total dissolved sulfide concentrations of <100 μM or burial of Mo initially delivered to the sediments through adsorption to Mn and/or Fe oxides. In the case of the sapropels at Landsort Deep—where Mo concentrations and Fe speciation indicate euxinia and the associated highly enriched Mn concentrations indicate likely widespread Mn-oxide burial—both of these possibilities are likely. As such, it is difficult to distinguish between two processes with overlapping fractionation relationships. Regardless, extreme Mn redox cycling relative to other modern anoxic settings as well as low water column dissolved sulfide concentrations and residence times are both consistent with dynamic redox conditions, such as those characterizing the modern Landsort Deep. This combination is our preferred interpretation for both of the euxinic sapropels and modern Landsort Deep sediments.

First, if water column total dissolved sulfide is <100 μM or only accumulates periodically, thus introducing kinetic challenges to quantitative tetrathiomolybdate formation (Erickson and Helz, 2000), a $\delta^{98}$Mo fractionation during conversion of molybdate to thiomolybdates can be captured in the sediments and can approach extreme fractionations from seawater of up to −3.1 permil (Azrieli-Tal and others, 2014). In contrast, when total dissolved sulfide concentrations are stable at levels >100 μM, as in the modern deep Black Sea, quantitative conversion of molybdate to tetrathiomolybdate occurs (Neubert and others, 2008). At the same time, near-quantitative water column Mo depletion is observed across the chemocline, with the net result that the $\delta^{98}$Mo of the sediments matches the ambient seawater (Barling and others, 2001; Arnold and others, 2004; Neubert and others, 2008). The $\delta^{98}$Mo range of both Landsort Deep euxinic sapropels, but particularly the upper sapropel, approach the most negative $\delta^{98}$Mo value (−0.7‰) predicted from previous efforts modeling of dissolved Mo speciation and isotope fractionations under extreme sulfide limitation (Azrieli-Tal and others, 2014). As such, our data are generally in the range anticipated with water column sulfide limitation inhibiting quantitative tetrathiomolybdate formation (fig. 6D). This conclusion is consistent with observations from the modern Landsort Deep where total dissolved sulfide values are observed below the 100 μM switchpoint that favors quantitative tetrathiomolybdate formation (Neubert and others, 2008; Nägler and others, 2011; Dellwig and others, 2012; Noordmann and others, 2015). Ultimately, oxygenated MBIs limit the timescales and concentration of water column sulfide accumulation within while simultaneously increasing the supply of dissolved molybdate to the Landsort Deep. As a result, vertical water column profiles show relatively little dissolved Mo depletion across the euxinic chemocline and modern sedimentary Mo isotope data range from −0.24 to +1.12 permil (Neubert and others, 2008; Nägler and others, 2011; Noordmann and others, 2015). Building on the suggestion from Mo-TOC ratios that Mo reservoir drawdown is not a major factor in the Baltic, the observed low $\delta^{98}$Mo values from all three Landsort Deep euxinic periods indicate that at no point in the past has the Landsort Deep been similar to more restricted modern euxinic basins where water column dissolved sulfide is stable at concentrations of hundreds of μM or higher (Algeo and Lyons, 2006).

Sorption of molybdate to Mn oxides provides an alternative, or in this case complementary, mechanism for transport of Mo to the sediments, especially considering the up to 15 weight percent Mn observed in the euxinic sapropels and the inferred oxidation of dissolved water column Mn during MBIs. There is an overlap in the $\delta^{98}$Mo fractionation during Mo sorption to Mn-oxides, −2.9 to −2.5 permil (Arnold and others, 2004; Wasylenki and others, 2008), and that associated with incomplete

conversion of molybdate to tetrathiomolybdate, which is potentially up to −3.1 permil (Azrieli-Tal and others, 2014). Following burial and reductive dissolution of the Mn oxides during diagenesis, quantitative conversion of molybdate to tetrathiomolybdate in sulfidic pore waters could then capture the negative isotope signature from oxide adsorption. The adsorption of Mo to Fe oxides and delivery to the sediments is also a relevant sedimentary Mo source. Oxidation of water column dissolve Fe could occur during MBIs or other redox oscillations, and adsorption of Mo to Fe oxides exerts large Mo isotope fractionations, ranging from −0.83 to −2.19 permil relative to the seawater signature depending on the specific Fe oxide mineralogy involved (Goldberg and others, 2009). Evidence that Fe and Mn oxide deposition is an important sedimentary Mo source even during euxinic sapropel deposition comes from similarities in $\delta^{98}$Mo data from the euxinic sapropels and those from intervals outside of the inferred euxinic layers (fig. 5). Molybdenum concentrations in the non-euxinic intervals are often greater than the 2 ppm crustal average but <25 ppm, indicating a likely oxide source for Mo transport to the sediments, which is subsequently sequestered upon reaction with pore water dissolved sulfide and organic carbon (Scott and Lyons, 2012).

A clear trend in the $\delta^{98}$Mo toward more negative values is observed moving upward within the brackish portion of the profile (fig. 5D), with $\delta^{98}$Mo values shifting from a range of +0.10 to +0.62 permil within the lower sapropel to +0.29 to −0.50 permil beginning directly above the lower sapropel (other than one outlier of +1.11‰). The $\delta^{98}$Mo range in the upper sapropel, −0.50 to −0.07 permil (again, barring one outlier), is distinctly more negative than in the lower sapropel (fig. 5D). Using our Mn concentration and Mo isotope data in combination with the known Mo isotope fractionations associated with Mo burial through both reaction with water column sulfide and adsorption to oxides, we can estimate the potential role of Mo delivered with Mn oxides versus Mo isotope fractionations during exposure to low and variable water column total dissolved sulfide concentrations of <100 μM. This exercise is not intended to quantify precisely the Mn versus euxinic sources of Mo but rather to demonstrate that their relative roles within the euxinic water columns during deposition of the two sapropels can be approximated. The following simple equation permits this mass balance approximation:

$$\delta^{98}\mathrm{Mo}_{\mathrm{sed}} = \delta^{98}\mathrm{Mo}_{\mathrm{eux}} \times (1 - f_{\mathbf{Mn}}) + \boldsymbol{\Delta}^{98}\mathrm{Mo}_{\mathrm{sw\text{-}ox}} \times f_{\mathbf{Mn}}. \quad (3)$$

Here, $\delta^{98}\mathrm{Mo}_{\mathrm{eux}}$ represents the sedimentary Mo isotope value following fractionation from seawater associated with non-quantitative tetrathiomolybdate conversion under euxinic conditions with low total dissolved sulfide concentrations (<100 μM), which, as mentioned, becomes progressively more negative relative to seawater with decreasing sulfide concentration and thus shorter residence time (Azrieli-Tal and others, 2014). The variable $f_{\mathbf{Mn}}$ represents the contribution of sedimentary Mo from Mn oxide relative to euxinic deposition. For simplicity, we choose to represent the Mo isotope fractionations related to Mn oxides ($\boldsymbol{\Delta}^{98}\mathrm{Mo}_{\mathrm{sw\text{-}ox}}$) as the maximum fractionation for Mo sorption to these oxide phases—that is, −2.9 permil from a seawater value of +2.4 permil. Maintaining a constant value for $\boldsymbol{\Delta}^{98}\mathrm{Mo}_{\mathrm{sw\text{-}ox}}$ is appropriate despite the known dynamic seawater conditions through the Baltic Holocene, as Mo isotope fractionations during adsorption to Mn oxides change little with the range of temperatures and salinities we can expect in this region (Wasylenki and others, 2008). Changes in the fraction of Fe versus Mn oxide Mo delivery to the sediments are also possible (Barling and Anbar, 2004; Wasylenki and others, 2008; Goldberg and others, 2009). Opposite to predictions from such variations, however, the upper sapropel has the highest Fe (now largely present as pyrite) and the most negative $\delta^{98}$Mo (fig. 5). Lastly, it could be assumed that a Mo flux to the sediments coupled to Mn oxides is substantial enough to deplete water column Mo. For our samples, this scenario is unlikely, as such

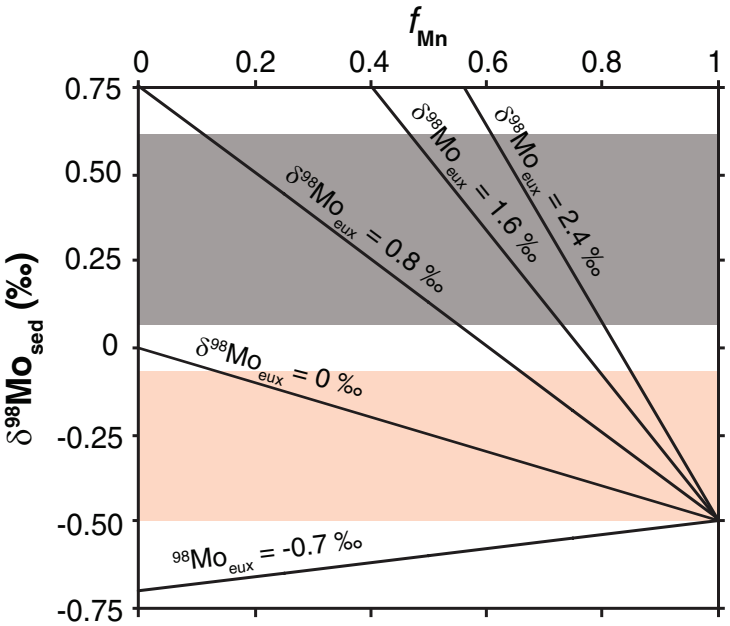


Fig. 7. Two end member-mixing model between sedimentary Mo ($\delta^{98}Mo_{sed}$) sourced from varied inputs of Mn-oxides ($f_{Mn}$) relative to euxinic deposition ($\delta^{98}Mo_{eux}$). Boxes are our measured $\delta^{98}Mo$ intervals from the sapropel intervals with the red representing the upper sapropel (barring one outlier) and the black the lower sapropel (fig. 5D). Justification and description of variables are given in the text. Sensitivity tests at varied $\delta^{98}Mo_{eux}$ represent progressive decreases in the concentration and residence of water column total dissolved sulfide at concentrations $<100$ μM.

a scenario would result in bulk sedimentary Mo isotope values closest to seawater in association with highest sedimentary Mn concentrations—the opposite of our observations (fig. 5).

Our model calculations demonstrate that the range in $\delta^{98}Mo$ from the lower sapropel cannot be explained by mixed Mn oxide and euxinic Mo burial if $\delta^{98}Mo_{eux}$ is approaching the lowest possible values of $-0.7$ permil as constrained from published modeling efforts (Azrieli-Tal and others, 2014) (fig. 7). We also observe that under no constant $\delta^{98}Mo_{eux}$ value does a simple doubling of $f_{Mn}$, as is observed from the lower to upper sapropel (fig. 5C), explain the shift in the $\delta^{98}Mo_{sed}$ values between the lower and upper sapropel without requiring Mn oxides as nearly the sole sedimentary Mo source in the upper scenario. A scenario demanding nearly all Mo as sourced from Mn oxides, and little from euxinic burial, is unlikely given our independent constraints on euxinic deposition in both sapropels based on Fe speciation, the Mo versus TOC relationship, and modern observations of euxinia at Landsort Deep. Instead, the relatively more negative $\delta^{98}Mo_{sed}$ in the upper sapropel likely requires more negative $\delta^{98}Mo_{eux}$ values along with increased $f_{Mn}$ compared to the lower sapropel. Decreases in $\delta^{98}Mo_{eux}$ point to a decrease in the absolute concentration and residence time of dissolved sulfide in the water column during deposition of the upper relative to lower sapropel. Considering that both extreme Mn redox cycling and low dissolved sulfide concentrations and residence times are consistent with dynamic redox conditions, we suggest that both of these factors likely contributed to the more negative $\delta^{98}Mo$ range observed in the upper euxinic sapropel compared to the lower. Ultimately, relatively more positive $\delta^{98}Mo$, lower Mn concentrations, and lower $Fe_T/Al$ in the lower sapropel

support more expansive and stable euxinia at Landsort Deep and likely the Baltic generally during the HTM relative to the MCA.

### *Modern and Past Anoxia Comparison*

Given the framework from previous studies of Fe, Mn, and Mo from sediments capturing the current euxinic period at Landsort Deep, we can further compare all three main Holocene Baltic anoxic events in the context of their relative stability and extent of reducing conditions. Figure 5 presents $Fe_T/Al$, Mn, Mo, and $\delta^{98}Mo$ data from the upper 15 cm of Landsort Deep published by Noordman and others (2015) (upper red dots), which includes the transition to the current euxinic era not captured in our study. Overall, the data suggest that the modern euxinic era represents a distinct redox state relative to the past euxinic periods. Modern Mn concentrations are as high as 18.8 weight percent and generally in the range >8 weight percent, and $\delta^{98}Mo$ ranges from −0.24 to +1.12 permil but is generally <0.29 permil. Similar to our interpretation of the upper sapropel (MCA), the high Mn concentrations and distinctly more negative $\delta^{98}Mo$ suggest that the current euxinic period has lower sulfide concentrations and residence times in the water column compared to HTM, the earliest euxinic interval captured in our core. Our interpretations of relatively higher and more stable sulfide concentrations at Landsort Deep during the HTM than today may also extend to other portions of the Baltic. In the Bothnian Sea, sedimentary Mo enrichments from the HTM are consistent with euxinia, while the modern Bothnian Sea is oxic. (Jilbert and others, 2015), supporting the conclusion that euxinic conditions were most expansive during the HTM. Ultimately, this comparison implies that despite a rapid expansion of anoxia in the modern Baltic relative to the anoxic periods of the past (Jilbert and Slomp, 2013), the current anoxic period at Landsort Deep may not yet have reached its maximum reducing potential if past events are a reliable guide.

## SUMMARY AND CONCLUSION

Following the most recent transition from lacustrine-to-brackish deposition, the lamination record at Landsort Deep indicates a generally anoxic water column persistently to the present, while the results of combined Fe, Mn, and Mo geochemistry provide evidence for multiple transitions between euxinic, ferruginous, and less reducing conditions. Euxinic deposition is clearly represented within two sapropel intervals with TOC contents of up to 8 weight percent. Highly enriched Mn concentrations throughout most of the brackish profile, but within the sapropels in particular, indicate that oxygenated and saline massive Baltic inflows from the North Sea commonly disrupted anoxic deposition throughout the past, similar to what we observe today (Carstensen and others, 2014). A comparison of $Fe_T/Al$, Mn, Mo, and $\delta^{98}Mo$ data from both sapropels to sedimentary data from the current Landsort Deep (Neubert and others, 2008; Lenz and others, 2014; Noordmann and others, 2015) indicate that euxinic water column conditions during the Holocene Thermal Maximum was most stable and likely the most reducing over the course of the Holocene.

Though our results clearly demonstrate potential variations in the strength of reducing conditions at Landsort Deep specifically, our Mo data also indicate that past euxinia has never approached the high and stable sulfide concentrations observed in other modern euxinic basins, such as the Black Sea. As we see in the Baltic today, there is a stratigraphic overlap between the indications of the most reducing conditions, as recorded in Fe speciation and Mo concentration data, and signatures of redox oscillations expressed through Mn concentrations and Mo isotopes. This seemingly contradictory temporal relationship is likely a result of both more expansive anoxia in the Baltic generally during these periods but with major Baltic inflows (MBIs) of North Sea saline and oxygen-rich waters acting to provide punctuated and short-lived replacement of formerly anoxic bottom waters. MBIs simultaneously strengthen the

halocline through input of marine North Sea water to brackish Baltic Sea bottom waters, providing the stratified water-column conditions necessary for maintenance of long-term Baltic anoxia. Though our records indicate variations in Baltic water column redox throughout the Holocene, the dual effect from MBIs of short-term oxidation of anoxic bottom waters and sustaining long-term anoxia implies that, as in the past, the future Baltic is unlikely to reach the reducing conditions observed in more restricted modern basins. As such, the unique expressions of Fe, Mn, and Mo geochemistry observed here and elsewhere in the Baltic Sea are characteristically different from more restricted modern euxinic basins and provide another euxinic example that can be extended to similar basins and redox controls through the geologic record.

ACKNOWLEDGMENTS

We would like to thank the captain and crew of the R/V Greatship Manisha, the Integrated Ocean Discovery Program, European Consortium for Ocean Research Drilling, as well as the scientific party of IODP expedition 347. DSH would like to thank the U.S. Science Support Program for providing a Schlanger Ocean Drilling Fellowship as support for the duration of this project. TL also acknowledges support from the NASA Astrobiology Institute via the UCR-led Alternative Earths Team. NR acknowledges support by the NASA Astrobiology Institute Postdoctoral Program, the U.S. Science Support program, and the National Science Foundation (NSF OCE-1234778 to NR and TL). For laboratory assistance crucial to this project, we thank Steve Bates, Terry Tang, and members of the Lyons and Planavsky laboratories of UCR and Yale. DSH thanks Sophie Green for providing Baltic bathymetric map. This manuscript benefited greatly from the reviews of E. Ingall, P. Kraal, and one anonymous reviewer.

REFERENCES

Algeo, T. J., and Lyons, T. W., 2006, Mo–total organic carbon covariation in modern anoxic marine environments: Implications for analysis of paleoredox and paleohydrographic conditions: Paleoceanography, v. 21, n. 1, PA1016, http://dx.doi.org/10.1029/2004PA001112

Andrén, T., and Sohlenius, G., 1995, Late Quaternary development of the north-western Baltic Proper—Results from the clay-varve investigation: Quaternary International, v. 27, p. 5–10, http://dx.doi.org/10.1016/1040-6182(94)00055-A

Andrén, E., Andrén, T., and Kunzendorf, H., 2000a, Holocene history of the Baltic Sea as a background for assessing records of human impact in the sediments of the Gotland Basin: The Holocene, v. 10, n. 6, p. 687–702, http://dx.doi.org/10.1191/09596830094944

Andrén, E., Andrén, T., and Sohlenius, G., 2000b, The Holocene history of the southwestern Baltic Sea as reflected in a sediment core from the Bornholm Basin: Boreas, v. 29, n. 3, p. 233–250, http://dx.doi.org/10.1111/j.1502-3885.2000.tb00981.x

Andrén, E., Clarke, A., Telford, R., Weckström, K., Vilbaste, S., Aigars, J., Conley, D., Johnsen, T., Juggins, S. and Korhola, A., 2007, Defining reference conditions for coastal areas in the Baltic Sea: Copenhagen, Denmark, Nordic Council of Ministers, TemaNord, 81 p., http://dx.doi.org/10.6027/09086692

Andrén, T., Björck, S., Andrén, E., Conley, D., Zillén, L., and Anjar, J., 2011, The development of the Baltic Sea Basin during the last 130 ka, *in* Harff, J., Björck, J., and Hoth, P., editors, The Baltic Sea Basin: Berlin, Springer, Central and Eastern European Development Studies (CEEDES), p. 75–97, http://dx.doi.org/10.1007/978-3-642-17220-5_4

Andrén, T., Jørgensen, B. B., Cotterill, C., Green, S., Andrén, E., Ash, J., Bauersachs, T., Cragg, B., Fanget, A.-S., Fehr, A., Granoszewski, W., Groeneveld, J., Hardisty, D., Herrero-Bervera, E., Hyttinen, O., Jensen, J. B., Johnson, S., Kenzler, M., Kotilainen, A., Kotthoff, U., Marshall, I. P. G., Martin, E., Obrochta, S., Passchier, S., Quintana Krupinski, N., Riedinger, N., Slomp, C., Snowball, I., Stepanova, A., Strano, S., Torti, A., Warnock, J., Xiao, N., and Zhang, R., 2015, Site M0063, *in* Andrén, T., Jørgensen, B.B., Cotterill, C., Green, S., and the Expedition 347 Scientists, Proceedings for the Integrated Ocean Drilling Program, v. 347: College Station, Texas (Integrated Ocean Drilling Program), http://dx.doi.org/10.2204/iodp.proc.347.107.2015

Arnold, G. L., Anbar, A. D., Barling, J., and Lyons, T. W., 2004, Molybdenum isotope evidence for widespread anoxia in mid-Proterozoic oceans: Science, v. 304, n. 5667, p. 87–90, http://dx.doi.org/10.1126/science.1091785

Asael, D., Tissot, F. L. H., Reinhard, C. T., Rouxel, O., Dauphas, N., Lyons, T. W., Ponzevera, E., Liorzou, C., and Chéron, S., 2013, Coupled molybdenum, iron and uranium stable isotopes as oceanic paleoredox proxies during the Paleoproterozoic Shunga Event: Chemical Geology, v. 362, p. 193–210, http://dx.doi.org/10.1016/j.chemgeo.2013.08.003

Azrieli-Tal, I., Matthews, A., Bar-Matthews, M., Almogi-Labin, A., Vance, D., Archer, C., and Teutsch, N.,

2014, Evidence from molybdenum and iron isotopes and molybdenum–uranium covariation for sulphidic bottom waters during Eastern Mediterranean sapropel S1 formation: Earth and Planetary Science Letters, v. 393, p. 231–242, http://dx.doi.org/10.1016/j.epsl.2014.02.054

Barling, J., and Anbar, A. D., 2004, Molybdenum isotope fractionation during adsorption by manganese oxides: Earth and Planetary Science Letters, v. 217, n. 3–4, p. 315–329, http://dx.doi.org/10.1016/S0012-821X(03)00608-3

Barling, J., Arnold, G. L. and Anbar, A. D., 2001, Natural mass-dependent variations in the isotopic composition of molybdenum: Earth and Planetary Science Letters, v. 193, n. 3–4, p. 447–457, http://dx.doi.org/10.1016/S0012-821X(01)00514-3

Berglund, B. E., Sandgren, P., Barnekow, L., Hannon, G., Jiang, H., Skog, G., and Yu, S.-Y., 2005, Early Holocene history of the Baltic Sea, as reflected in coastal sediments in Blekinge, southeastern Sweden: Quaternary International, v. 130, n. 1, p. 111–139, http://dx.doi.org/10.1016/j.quaint.2004.04.036

Berner, R. A., 1982, Burial of organic carbon and pyrite sulfur in the modern ocean: Its geochemical and environmental significance: American Journal of Science, v. 282, n. 4, p. 451–473, http://dx.doi.org/10.2475/ajs.282.4.451

_____ 1984, Sedimentary pyrite formation: An update: Geochimica et Cosmochimica Acta, v. 48, n. 4, p. 605–615, http://dx.doi.org/10.1016/0016-7037(84)90089-9

Berner, R. A., and Raiswell, R., 1983, Burial of organic carbon and pyrite sulfur in sediments over Phanerozoic time: A new theory: Geochimica et Cosmochimica Acta, v. 47, n. 3, p. 855–862, http://dx.doi.org/10.1016/0016-7037(83)90151-5

Berner, R. A., Baldwin, T., and Holdren, G. R., Jr., 1979, Authigenic iron sulfides as paleosalinity indicators: Journal of Sedimentary Research, v. 49, n. 4, p. 1345–1350, http://dx.doi.org/10.1306/212F7923-2B24-11D7-8648000102C1865D

Björck, S., 2008, The late Quaternary development of the Baltic Sea basin, *in* The BACC Author Team, editors, Assessment of climate change for the Baltic Sea Basin: Berlin, Springer, p. 398–407.

Björck, S., Kromer, B., Johnsen, S., Bennike, O., Hammarlund, D., Lemdahl, G., Possnert, G., Rasmussen, T. L., Wohlfarth, B., Hammer, C. U., and Spurk, M., 1996, Synchronized Terrestrial-Atmospheric Deglacial Records Around the North Atlantic: Science, v. 274, n. 5290, p. 1155–1160, http://dx.doi.org/10.1126/science.274.5290.1155

Björck, S., Andrén, T. and Jensen, J. B., 2008, An attempt to resolve the partly conflicting data and ideas on the Ancylus-Littorina transition, *in* Proceedings of the Workshop "Relative sea level changes": Polish Geological Institute Special Papers, v. 23, p. 21–26.

Boesen, C., and Postma, D., 1988, Pyrite formation in anoxic environments of the Baltic: American Journal of Science, v. 288, n. 6, p. 575–603, http://dx.doi.org/10.2475/ajs.288.6.575

Canfield, D. E., Raiswell, R., Westrich, J. T., Reaves, C. M., and Berner, R. A., 1986, The use of chromium reduction in the analysis of reduced inorganic sulfur in sediments and shales: Chemical Geology, v. 54, n. 1–2, p. 149–155, http://dx.doi.org/10.1016/0009-2541(86)90078-1

Canfield, D. E., Raiswell, R., and Bottrell, S. H., 1992, The reactivity of sedimentary iron minerals toward sulfide: American Journal of Science, v. 292, n. 9, p. 659–683, http://dx.doi.org/10.2475/ajs.292.9.659

Canfield, D. E., Lyons, T. W., and Raiswell, R., 1996, A model for iron deposition to euxinic Black Sea sediments: American Journal of Science, v. 296, n. 7, p. 818–834, http://dx.doi.org/10.2475/ajs.296.7.818

Canfield, D. E., Poulton, S. W., Knoll, A. H., Narbonne, G. M., Ross, G., Goldberg, T., and Strauss, H., 2008, Ferruginous conditions dominated later Neoproterozoic deep-water chemistry: Science, v. 321, n. 5891, p. 949–952, http://dx.doi.org/10.1126/science.1154499

Carstensen, J., Andersen, J. H., Gustafsson, B. G., and Conley, D. J., 2014, Deoxygenation of the Baltic Sea during the last century: Proceedings of the National Academy of Sciences of the United States of America, v. 111, n. 15, p. 5628–5633, http://dx.doi.org/10.1073/pnas.1323156111

Chanton, J. P., and Martens, C. S., 1985, The effects of heat and stannous chloride addition on the active distillation of acid volatile sulfide from pyrite-rich marine sediment samples: Biogeochemistry, v. 1, n. 4, p. 375–382, http://dx.doi.org/10.1007/BF02187379

Cline, J. D., 1969, Spectrophotometric determination of hydrogen sulfide in natural waters: Limnology and Oceanography, v. 14, n. 3, p. 454–458, http://dx.doi.org/10.4319/lo.1969.14.3.0454

Conley, D. J., Björck, S., Bonsdorff, E., Carstensen, J., Destouni, G., Gustafsson, B. G., Hietanen, S., Kortekaas, M., Kuosa, H., Markus Meier, H., Müller-Karulis, B., Nordberg, K., Norkko, A., Nürnberg, G., Pitkänen, H., Rabalais, N. N., Rosenberg, R., Savchuk, O. P., Slomp, C. P., Voss, M., Wulff, F., and Zillén, L., 2009, Hypoxia-related processes in the Baltic Sea: Environmental Science & Technology, v. 43, n. 10, p. 3412–3420, http://dx.doi.org/10.1021/es802762a

Dahl, T. W., Chappaz, A., Fitts, J. P., and Lyons, T. W., 2013, Molybdenum reduction in a sulfidic lake: Evidence from X-ray absorption fine-structure spectroscopy and implications for the Mo paleoproxy: Geochimica et Cosmochimica Acta, v. 103, p. 213–231, http://dx.doi.org/10.1016/j.gca.2012.10.058

Dashtgard, S. E., and MacEachern, J. A., 2016, Unburrowed mudstones may record only slightly lowered oxygen conditions in warm, shallow basins: Geology, v. 44, n. 5, p. 371–374, http://dx.doi.org/10.1130/G37648.1

Dellwig, O., Schnetger, B., Brumsack, H.-J., Grossart, H.-P. and Umlauf, L., 2012, Dissolved reactive manganese at pelagic redoxclines (part II): Hydrodynamic conditions for accumulation: Journal of Marine Systems, v. 90, n. 1, p. 31–41, http://dx.doi.org/10.1016/j.jmarsys.2011.08.007

Diaz, R. J., and Rosenberg, R., 2008, Spreading dead zones and consequences for marine ecosystems: Science, v. 321, n. 5891, p. 926–929, http://dx.doi.org/10.1126/science.1156401

Döös, K., Meier, H. E. M., and Döscher, R., 2004, The Baltic haline conveyor belt or the overturning circulation and mixing in the Baltic: AMBIO: A Journal of the Human Environment, v. 33, n. 4, p. 261–266, http://dx.doi.org/10.1579/0044-7447-33.4.261

Erickson, B. E., and Helz, G. R., 2000, Molybdenum (VI) speciation in sulfidic waters: Stability and lability of thiomolybdates: Geochimica et Cosmochimica Acta, v. 64, n. 7, p. 1149–1158, http://dx.doi.org/10.1016/S0016-7037(99)00423-8

Fehr, M. A., Andersson, P. S., Hålenius, U., and Mörth, C.-M., 2008, Iron isotope variations in Holocene sediments of the Gotland Deep, Baltic Sea: Geochimica et Cosmochimica Acta, v. 72, n. 3, p. 807–826, http://dx.doi.org/10.1016/j.gca.2007.11.033

Ferdelman, T. G., ms, 1988, The distribution of sulfur, iron, manganese, copper and uranium in a salt marsh sediment core as determined by a sequential extraction method: Newark, Delaware, University of Delaware, M. S. thesis, 244 p.

Goldberg, T., Archer, C., Vance, D., and Poulton, S. W., 2009, Mo isotope fractionation during adsorption to Fe (oxyhydr) oxides: Geochimica et Cosmochimica Acta, v. 73, n. 21, p. 6502–6516, http://dx.doi.org/10.1016/j.gca.2009.08.004

Goldschmidt, V., 1933, Grundlagen der quantitativen Geochemie: Fortschritte der Mineralogie, Kristallographie und Petrographie, v. 17, p. 112.

Gustafsson, B. G., and Westman, P., 2002, On the causes for salinity variations in the Baltic Sea during the last 8500 years: Paleoceanography, v. 17, n. 3, p. 12-11–12-14, http://dx.doi.org/10.1029/2000PA000572

Houmark-Nielsen, M., and Henrik Kjær, K., 2003, Southwest Scandinavia, 40–15 kyr BP: Palaeogeography and environmental change: Journal of Quaternary Science, v. 18, n. 8, p. 769–786, http://dx.doi.org/10.1002/jqs.802

Hurtgen, M. T., Lyons, T. W., Ingall, E. D., and Cruse, A. M., 1999, Anomalous enrichments of iron monosulfide in euxinic marine sediments and the role of $H_2S$ in iron sulfide transformations: Examples from Effingham Inlet, Orca Basin, and the Black Sea: American Journal of Science, v. 299, n. 7–9, p. 556–588, http://dx.doi.org/10.2475/ajs.299.7-9.556

Jakobsson, M., Björck, S., Alm, G., Andrén, T., Lindeberg, G., and Svensson, N.-O., 2007, Reconstructing the Younger Dryas ice dammed lake in the Baltic Basin: Bathymetry, area and volume: Global and Planetary Change, v. 57, n. 3–4, p. 355–370, http://dx.doi.org/10.1016/j.gloplacha.2007.01.006

Jilbert, T., and Slomp, C. P., 2013, Rapid high-amplitude variability in Baltic Sea hypoxia during the Holocene: Geology, v. 41, n. 11, p. 1183–1186, http://dx.doi.org/10.1130/G34804.1

Jilbert, T., Conley, D. J., Gustafsson, B. G., Funkey, C. P., and Slomp, C. P., 2015, Glacio-isostatic control on hypoxia in a high-latitude shelf basin: Geology, v. 43, n. 5, p. 427–430, http://dx.doi.org/10.1130/G36454.1

Kabel, K., Moros, M., Porsche, C., Neumann, T., Adolphi, F., Andersen, T. J., Siegel, H., Gerth, M., Leipe, T., Jansen, E., and Sinninghe Damsté, J. S., 2012, Impact of climate change on the Baltic Sea ecosystem over the past 1,000 years: Nature Climate Change, v. 2, p. 871–874, http://dx.doi.org/10.1038/nclimate1595

Kostka, J. E., and Luther, G. W., III, 1994, Partitioning and speciation of solid phase iron in saltmarsh sediments: Geochimica et Cosmochimica Acta, v. 58, n. 7, p. 1701–1710, http://dx.doi.org/10.1016/0016-7037(94)90531-2

Lambeck, K., and Chappell, J., 2001, Sea level change through the last glacial cycle: Science, v. 292, n. 5517, p. 679–686, http://dx.doi.org/10.1126/science.1059549

Lenz, C., Jilbert, T., Conley, D., Wolthers, M., and Slomp, C., 2014, Are recent changes in sediment manganese sequestration in the euxinic basins of the Baltic Sea linked to the expansion of hypoxia?: Biogeosciences Discussions, v. 11, p. 9889–9918, http://dx.doi.org/10.5194/bgd-11-9889-2014

Lenz, C., Jilbert, T., Conley, D. J., and Slomp, C. P., 2015, Hypoxia - driven variations in iron and manganese shuttling in the Baltic Sea over the past 8 kyr: Geochemistry, Geophysics, Geosystems, v. 16, n. 10, p. 3754–3766, http://dx.doi.org/10.1002/2015GC005960

Lepland, A., and Stevens, R. L., 1998, Manganese authigenesis in the Landsort Deep, Baltic Sea: Marine Geology, v. 151, n. 1–4, p. 1–25, http://dx.doi.org/10.1016/S0025-3227(98)00046-2

Lyons, T. W., 1997, Sulfur isotopic trends and pathways of iron sulfide formation in upper Holocene sediments of the anoxic Black Sea: Geochimica et Cosmochimica Acta, v. 61, n. 16, p. 3367–3382, http://dx.doi.org/10.1016/S0016-7037(97)00174-9

Lyons, T. W., and Severmann, S., 2006, A critical look at iron paleoredox proxies: New insights from modern euxinic marine basins: Geochimica et Cosmochimica Acta, v. 70, n. 23, p. 5698–5722, http://dx.doi.org/10.1016/j.gca.2006.08.021

Matthäus, W., 2006, The History of Investigation of Salt Water Inflows Into the Baltic Sea: From Early Beginning to Recent Results: Institut für Ostseeforschung Warnemünde, Marine Science Reports, n. 65, 81 p.

Middelburg, J. J., 1991, Organic carbon, sulphur, and iron in recent semi-euxinic sediments of Kau Bay, Indonesia: Geochimica et Cosmochimica Acta, v. 55, n. 3, p. 815–828, http://dx.doi.org/10.1016/0016-7037(91)90344-5

Miller, C. A., Peucker-Ehrenbrink, B., Walker, B. D., and Marcantonio, F., 2011, Re-assessing the surface cycling of molybdenum and rhenium: Geochimica et Cosmochimica Acta, v. 75, n. 22, p. 7146–7179, http://dx.doi.org/10.1016/j.gca.2011.09.005

Mohrholz, V., Naumann, M., Nausch, G., Krüger, S., and Gräwe, U., 2015, Fresh oxygen for the Baltic Sea—An exceptional saline inflow after a decade of stagnation: Journal of Marine Systems, v. 148, p. 152–166, http://dx.doi.org/10.1016/j.jmarsys.2015.03.005

Morse, J. W., and Cornwell, J. C., 1987, Analysis and distribution of iron sulfide minerals in recent anoxic marine sediments: Marine Chemistry, v. 22, n. 1, p. 55–69, http://dx.doi.org/10.1016/0304-4203(87)90048-X

Nägler, T. F., Neubert, N., Böttcher, M. E., Dellwig, O., and Schnetger, B., 2011, Molybdenum isotope fractionation in pelagic euxinia: Evidence from the modern Black and Baltic Seas: Chemical Geology, v. 289, n. 1–2, p. 1–11, http://dx.doi.org/10.1016/j.chemgeo.2011.07.001

Nägler, T. F., Anbar, A. D., Archer, C., Goldberg, T., Gordon, G. W., Greber, N. D., Siebert, C., Sohrin, Y., and Vance, D., 2014, Proposal for an international molybdenum isotope measurement standard and data representation: Geostandards and Geoanalytical Research, v. 38, n. 2, p. 149–151, http://dx.doi.org/10.1111/j.1751-908X.2013.00275.x

Neubert, N., Nägler, T. F., and Böttcher, M. E., 2008, Sulfidity controls molybdenum isotope fractionation into euxinic sediments: Evidence from the modern Black Sea: Geology, v. 36, n. 10, p. 775–778, http://dx.doi.org/10.1130/G24959A.1

Noordmann, J., Weyer, S., Montoya-Pino, C., Dellwig, O., Neubert, N., Eckert, S., Paetzel, M. and Böttcher, M., 2015, Uranium and molybdenum isotope systematics in modern euxinic basins: Case studies from the central Baltic Sea and the Kyllaren fjord (Norway): Chemical Geology, v. 396, p. 182–195, http://dx.doi.org/10.1016/j.chemgeo.2014.12.012

Parkhurst, D. L., and Appelo, C. A. J., 1999, User's guide to PHREEQC (Version 2): A computer program for speciation, batch-reaction, one-dimensional transport, and inverse geochemical calculations: Denver, Colorado, U.S. Geological Survey, Water-Resources Investigations Report 99-4259, 312 p.

Poulton, S. W., and Canfield, D. E., 2005, Development of a sequential extraction procedure for iron: Implications for iron partitioning in continentally derived particulates: Chemical Geology, v. 214, n. 3–4, p. 209–221, http://dx.doi.org/10.1016/j.chemgeo.2004.09.003

_____ 2011, Ferruginous conditions: A dominant feature of the ocean through Earth's history: Elements, v. 7, n. 2, p. 107–112, http://dx.doi.org/10.2113/gselements.7.2.107

Raiswell, R., and Anderson, T. F., 2005, Reactive iron enrichment in sediments deposited beneath euxinic bottom waters: Constraints on supply by shelf recycling: Geological Society, London, Special Publications, v. 248, p. 179–194, http://dx.doi.org/10.1144/GSL.SP.2005.248.01.10

Raiswell, R., and Canfield, D. E., 1998, Sources of iron for pyrite formation in marine sediments: American Journal of Science, v. 298, n. 3, p. 219–245, http://dx.doi.org/10.2475/ajs.298.3.219

Raiswell, R., Canfield, D. E., and Berner, R. A., 1994, A comparison of iron extraction methods for the determination of degree of pyritisation and the recognition of iron-limited pyrite formation: Chemical Geology, v. 111, n. 1–4, p. 101–110, http://dx.doi.org/10.1016/0009-2541(94)90084-1

Raiswell, R., Vu, H. P., Brinza, L., and Benning, L. G., 2010, The determination of labile Fe in ferrihydrite by ascorbic acid extraction: Methodology, dissolution kinetics and loss of solubility with age and dewatering: Chemical Geology, v. 278, n. 1–2, p. 70–79, http://dx.doi.org/10.1016/j.chemgeo.2010.09.002

Scholz, F., McManus, J., and Sommer, S., 2013, The manganese and iron shuttle in a modern euxinic basin and implications for molybdenum cycling at euxinic ocean margins: Chemical Geology, v. 355, p. 56–68, http://dx.doi.org/10.1016/j.chemgeo.2013.07.006

Scholz, F., Severmann, S., McManus, J., and Hensen, C., 2014, Beyond the Black Sea paradigm: The sedimentary fingerprint of an open-marine iron shuttle: Geochimica et Cosmochimica Acta, v. 127, p. 368–380, http://dx.doi.org/10.1016/j.gca.2013.11.041

Scott, C., and Lyons, T. W., 2012, Contrasting molybdenum cycling and isotopic properties in euxinic versus non-euxinic sediments and sedimentary rocks: Refining the paleoproxies: Chemical Geology, v. 324–325, p. 19–27, http://dx.doi.org/10.1016/j.chemgeo.2012.05.012

Siebert, C., Nägler, T. F., von Blanckenburg, F., and Kramers, J. D., 2003, Molybdenum isotope records as a potential new proxy for paleoceanography: Earth and Planetary Science Letters, v. 211, n. 1–2, p. 159–171, http://dx.doi.org/10.1016/S0012-821X(03)00189-4

Sohlenius, G., and Westman, P., 1998, Salinity and redox alternations in the northwestern Baltic proper during the late Holocene: Boreas, v. 27, n. 2, p. 101–114 http://dx.doi.org/10.1111/j.1502-3885.1998.tb00871.x

Sohlenius, G., Sternbeck, J., Andrén, E., and Westman, P., 1996, Holocene history of the Baltic Sea as recorded in a sediment core from the Gotland Deep: Marine Geology, v. 134, n. 3–4, p. 183–201, http://dx.doi.org/10.1016/0025-3227(96)00047-3

Sohlenius, G., Emeis, K.-C., Andrén, E., Andrén, T., and Kohly, A., 2001, Development of anoxia during the Holocene fresh–brackish water transition in the Baltic Sea: Marine Geology, v. 177, n. 3–4, p. 221–242, http://dx.doi.org/10.1016/S0025-3227(01)00174-8

Sternbeck, J., and Sohlenius, G., 1997, Authigenic sulfide and carbonate mineral formation in Holocene sediments of the Baltic Sea: Chemical Geology, v. 135, n. 1–2, p. 55–73, http://dx.doi.org/10.1016/S0009-2541(96)00104-0

Sternbeck, J., Sohlenius, G. and Hallberg, R. O., 2000, Sedimentary trace elements as proxies to depositional changes induced by a Holocene fresh-brackish water transition: Aquatic Geochemistry, v. 6, n. 3, p. 325–345, http://dx.doi.org/10.1023/A:1009680714930

Stigebrandt, A., and Gustafsson, B. G., 2003, Response of the Baltic Sea to climate change—theory and observations: Journal of Sea Research, v. 49, n. 4, p. 243–256, http://dx.doi.org/10.1016/S1385-1101(03)00021-2

Suess, E., 1979, Mineral phases formed in anoxic sediments by microbial decomposition of organic matter: Geochimica et Cosmochimica Acta, v. 43, n. 3, p. 339–352, http://dx.doi.org/10.1016/0016-7037(79)90199-6

Tossell, J. A., 2005, Calculating the partitioning of the isotopes of Mo between oxidic and sulfidic species in aqueous solution: Geochimica et Cosmochimica Acta, v. 69, n. 12, p. 2981–2993, http://dx.doi.org/10.1016/j.gca.2005.01.016

Turekian, K. K., and Wedepohl, K. H., 1961, Distribution of the elements in some major units of the earth's crust: Geological Society of America Bulletin, v. 72, n. 2, p. 175–192, http://dx.doi.org/10.1130/0016-7606(1961)72[175:DOTEIS]2.0.CO;2

Walker, M., Johnsen, S., Rasmussen, S. O., Popp, T., Steffensen, J. P., Gibbard, P., Hoek, W., Lowe, J., Andrews, J., Björck, S., Cwynar, L. C., Hughen, K., Kershaw, P., Kromer, B., Litt, T., Lowe, D. J., Nakagawa, T., Newnham, R., and Schwander, J., 2009, Formal definition and dating of the GSSP (Global

Stratotype Section and Point) for the base of the Holocene using the Greenland NGRIP ice core, and selected auxiliary records: Journal of Quaternary Science, v. 24, n. 1, p. 3–17, http://dx.doi.org/10.1002/jqs.1227

Wastegård, S., Andrén, T., Sohlenius, G., and Sandgren, P., 1995, Different phases of the Yoldia Sea in the north-western Baltic Proper: Quaternary International, v. 27, p. 121–129, http://dx.doi.org/10.1016/1040-6182(94)00069-H

Wasylenki, L. E., Rolfe, B. A., Weeks, C. L., Spiro, T. G., and Anbar, A. D., 2008, Experimental investigation of the effects of temperature and ionic strength on Mo isotope fractionation during adsorption to manganese oxides: Geochimica et Cosmochimica Acta, v. 72, n. 24, p. 5997–6005, http://dx.doi.org/10.1016/j.gca.2008.08.027

Zillén, L., Conley, D. J., Andrén, T., Andrén, E., and Björck, S., 2008, Past occurrences of hypoxia in the Baltic Sea and the role of climate variability, environmental change and human impact: Earth-Science Reviews, v. 91, n. 1–4, p. 77–92, http://dx.doi.org/10.1016/j.earscirev.2008.10.001